NUCLEAR MAGNETIC RESONANCE FOURIER TRANSFORM SPECTROSCOPY

Nobel Lecture, December 9, 1992

by

RICHARD R. ERNST

Laboratorium für Physikalische Chemie, Eidgenössische Technische Hochschule, ETH-Zentrum 8092 Zurich, Switzerland

The world of the nuclear spins is a true paradise for theoretical and experimental physicists. It supplies, for example, most simple test systems for demonstrating the basic concepts of quantum mechanics and quantum statistics, and numerous textbook-like examples have emerged. On the other hand, the ease of handling nuclear spin systems predestinates them for testing novel experimental concepts. Indeed, the universal procedures of coherent spectroscopy have been developed predominantly within nuclear magnetic resonance (NMR) and have found widespread application in a variety of other fields.

Several key experiments of magnetic resonance have already been honored by physics Nobel prizes, starting with the famous molecular beam experiments by Isidor I. Rabi (1-3) acknowledged in 1944, followed by the classical NMR experiments by Edward M. Purcell (4) and Felix Bloch (5,6), honored with the 1952 prize, and the optical detection schemes by Alfred Kastler (7), leading to a prize in 1966. Some further physics Nobel prize winners have been associated in various ways with magnetic resonance: John H. Van Vleck developed the theory of dia- and paramagnetism and introduced the moment method into NMR, Nicolaas Bloembergen had a major impact on early relaxation theory and measurements; Karl Alex Müller has contributed significantly to electron paramagnetic resonance; Norman F. Ramsey is responsible for the basic theory of chemical shifts and J couplings; and Hans G. Dehmelt has developed pure nuclear quadrupole resonance.

But not only for physicists is nuclear magnetic resonance of great fascination. More and more chemists, biologists, and medical doctors discover NMR, not so much for its conceptual beauty but for its extraordinary usefulness. In this context, a great number of magnetic resonance tools have been invented to enhance the power of NMR in view of a variety of applications (8-15). This Nobel lecture provides a glimpse behind the scene of an NMR toolmaker's workshop.

Nuclear spin systems possess unique properties that predestinate them for molecular studies:

(i) The nuclear sensors provided by nature are extremely well localized, with a diameter of a few femtometers, and can report on local affairs in their immediate vicinity. It is thus possible to explore molecules and matter in great detail.

(ii) The interaction energy of the sensors with the environment is extremely small, with less than 0.2 J/mol, corresponding to the thermal energy at 30 mK, and the monitoring of molecular properties is virtually perturbation-free. Nevertheless, the interaction is highly sensitive to the local environment.

(iii) Geometrical information can be obtained from nuclear pair interactions. Magnetic dipolar interactions provide distance information, while scalar J-coupling interactions allow one to determine dihedral bond angles.

On first sight, it may be astonishing that it is possible to accurately determine internuclear distances by radio frequencies with wavelengths $\lambda \simeq 1$ m, that seemingly violate the quantum mechanical uncertainty relation, $\sigma_q \cdot \sigma_p \geq \hbar/2$, with the linear momentum $p = 2\pi h/\lambda$, as it applies to scattering experiments or to a microscope. It is important that in magnetic resonance the geometric information is encoded in the spin Hamiltonian, $\mathcal{H} = \mathcal{H}(\mathbf{q}_1, \ldots, \mathbf{q}_k)$, where $\mathbf{q}_k$ are the nuclear coordinates. An accurate geometric measurement, therefore, boils down to an accurate energy measurement that can be made as precise as desired, provided that the observation time t is extended according to $\sigma_E \cdot t \geq \hbar/2$. An upper limit of t is in practice given by the finite lifetime of the energy eigenstates due to relaxation processes. Thus, the accuracy of NMR measurements is not restricted by the wavelength but rather by relaxation-limited lifetimes.

The information content of a nuclear spin Hamiltonian and the associated relaxation superoperator of a large molecule, e.g. a protein, is immense. It is possible to determine the chemical shift frequencies of hundreds of spins in a molecule to an accuracy of 16-18 bits. Internuclear distances for thousands of proton pairs can be measured to about 0.1 A. Several hundred dihedral angles in a molecule can be determined with an uncertainty of less than 10°.

The weakness of the nuclear spin interactions, so far described as an advantage, leads on the other hand to severe detection problems. Large numbers of spins are required to discriminate the weak signals from noise. Under optimum conditions with modern high field NMR spectrometers, 10^{14}-10^{15} spins of one kind are needed to detect a signal within a performance time of one hour. The low signal-to-noise ratio is the most limiting handicap of NMR. Any increase by technical means will significantly extend the possible range of NMR applications.

This clearly defines the two goals that had to be achieved during the past three decades to promote NMR as a practical tool for molecular structure determination:

(i) Optimization of the signal-to-noise ratio.

(ii) Development of procedures to cope with the enormous amount of inherent molecular information.

ONE-DIMENSIONAL FOURIER TRANSFORM SPECTROSCOPY

A major improvement in the signal-to-noise ratio of NMR has been achieved in 1964 by the conception of Fourier transform spectroscopy. The basic principle, parallel data acquisition, leading to the multiplex advantage, was applied already by Michelson in 1891 for optical spectroscopy (16) and explicitly formulated by Fellgett in 1951 (17). However, the approach used in optics, spatial interferometry, is unsuited for NMR where an interferometer with the necessary resolution would require a path length of at least $3 \cdot 10^8$m.

Weston A. Anderson at Varian Associates, Palo Alto, was experimenting in the early sixties with a mechanical multiple frequency generator, the "wheel of fortune" that was conceived to simultaneously excite the spin system with N frequencies in order to shorten the performance time of an experiment by a factor N, recording the response of N spectral elements in parallel (18). It was soon recognized that more elegant solutions were needed for a commercial success.

Numerous possibilities are conceivable for the generation of a broad band frequency source that allows the simultaneous irradiation of an entire spectrum. We mention four schemes: (i) Radio frequency pulse excitation, (ii) stochastic random noise excitation, (iii) rapid scan excitation, (iv) excitation by a computer-synthesized multiple-frequency waveform. For each scheme, a different type of data processing is required to derive the desired NMR spectrum.

The application of radio frequency (rf) pulse excitation was suggested by Weston A. Anderson to the author for a detailed experimental study in 1964 (19-21). The experiment is explained in Fig. 1. To the sample that is polarized in a static magnetic field along the z-axis, an rf pulse is applied along the y-axis. It rotates the magnetization vectors M_k of all spins I_k by $\pi/2$ into an orientation perpendicular to the static field:

$$M_{kz} \xrightarrow{(\pi/2)_y} M_{kx}, \qquad [1]$$

using a convenient arrow notation (23) with the acting operator, here a $(\pi/2)_y$ rotation, on the top of the arrow. The following free induction decay (FID) consists of the superposition of all eigenmodes of the system. An observable operator D is used to detect the signal that is Fourier-transformed for separating the different spectral contributions. Figure 1 contains an early example of Fourier transform spectroscopy using the sample 7-ethoxy-4-methyl-coumarin of which 500 FID's were co-added and Fourier-transformed to produce the Fourier transform spectrum (FT) shown (22). A slow passage continuous wave spectrum (cw), recorded in the same total time of 500 s, is shown also in Fig. 1 for comparison of the signal-to-noise ratios.

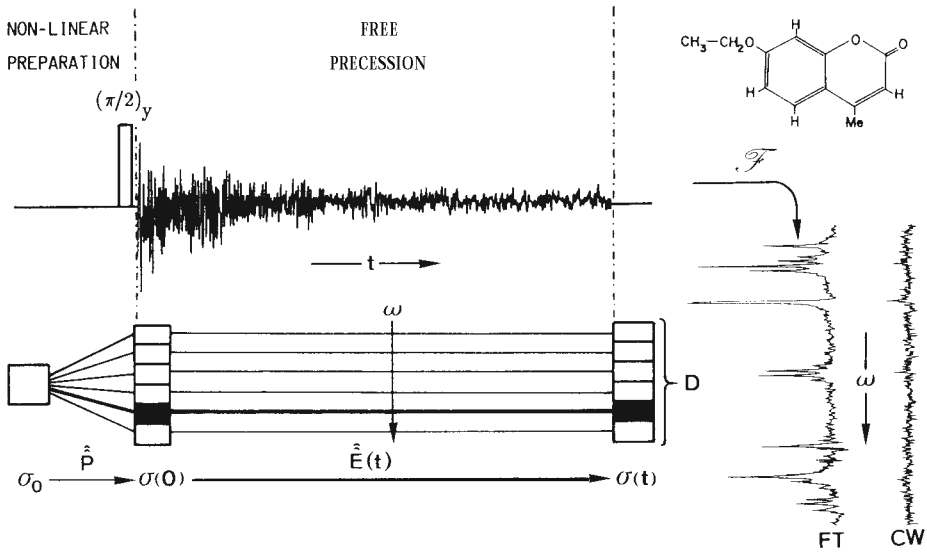

Figure 1. Schematic representation of pulse Fourier transform spectroscopy by the example of 60MHz proton resonance of 7-ethoxy-4-methyl-coumarin (22). An initial $(\pi/2)_y$ rf pulse, represented by the rotation superoperator P, excites from the equilibrium state σ_0 transverse magnetization $\sigma(0)$. Free precession of all coherences in parallel under the evolution superoperator E(t) leads to the final state $\sigma(t)$. Detection with the detection operator D produces the shown FID (sum of 500 scans) which, after Fourier transformation, produces the spectrum FT. For comparison, a continuous wave spectrum CW is shown that has been recorded in the same total time of 500 s under identical conditions.

To please the more mathematically inclined reader, the experiment can also be expressed by the evolution of the density operator $\sigma(t)$ under the preparation superoperator $\hat{\mathcal{P}} = \exp\{-i\hat{\mathcal{F}}_y\pi/2\}$ and the evolution superoperator $\hat{\mathcal{E}}(t) = \exp\{-i\hat{\mathcal{H}}t - \Gamma t\}$. The superoperator $\hat{\mathcal{F}}_y$ is defined by $\hat{\mathcal{F}}_y A = [F_y, A]$ with $F_y = \Sigma_k I_{ky}$ where I_{ky} is a component angular momentum operator of spink. $\hat{\mathcal{H}}$ is the Hamiltonian commutator superoperator, $\mathcal{H}A = [H,A]$, and $\hat{\Gamma}$ is the relaxation superoperator. The expectation value $< D > (t)$ of the observable operator D is then given by

$$< D > (t) = \mathrm{Tr}\{D\hat{\mathcal{E}}(t)\hat{\mathcal{P}}\sigma_0\} \qquad [2]$$

where σ_0 represents the thermal equilibrium density operator of the spin system.

The reduction in performance time is determined by the number of spectral elements N, i.e. the number of significant points in the spectrum, roughly given by $N = F/\Delta f$ where F is the total spectral width and Δf a typical signal line width. A corresponding increase in the signal-to-noise ratio of $\sqrt{N}$ per unit time can be obtained by co-adding an appropriate number of FID signals originating from a repetitive pulse experiment. The signal-to-noise gain can be appreciated from Fig. 1.

It has been known since a long time that the frequency response function (spectrum) of a linear system is the Fourier transform of the impulse

response (free induction decay). This was already implicitly evident in the work of Jean Baptiste Joseph Fourier who investigated in 1822 the heat conduction in solid bodies (24). Lowe and Norberg have proved in 1957 this relation also to hold for spin systems despite their strongly nonlinear response characteristics (25).

Stochastic testing of unknown systems by white random noise has been proposed in the 1940s by Norbert Wiener (26). So to say, the color of the output noise carries the spectral information on the investigated system. The first applications of random noise excitation in NMR have been proposed independently by Russel H.Varian (27) and by Hans Primas (28, 29), for broadband testing and for broadband decoupling, respectively. The first successful experiments using random noise irradiation led to heteronuclear "noise decoupling" (30, 31), a method that proved to be essential for the practical success of carbon-l 3 resonance in chemical applications.

In 1971, Reinhold Raiser (32) and the author (33) independently demonstrated stochastic resonance as a means to improve the signal-to-noise ratio of NMR by broadband irradiation. Here, the computed cross-correlation function

$$c_1(\tau) = n_o(t)\, n_i\, (t—\tau) \qquad [3]$$

of the input noise $n_i(t)$ and the output noise $n_o(t)$ is equivalent to the FID of pulse Fourier transform spectroscopy. This is illustrated in Fig.2 for flu-

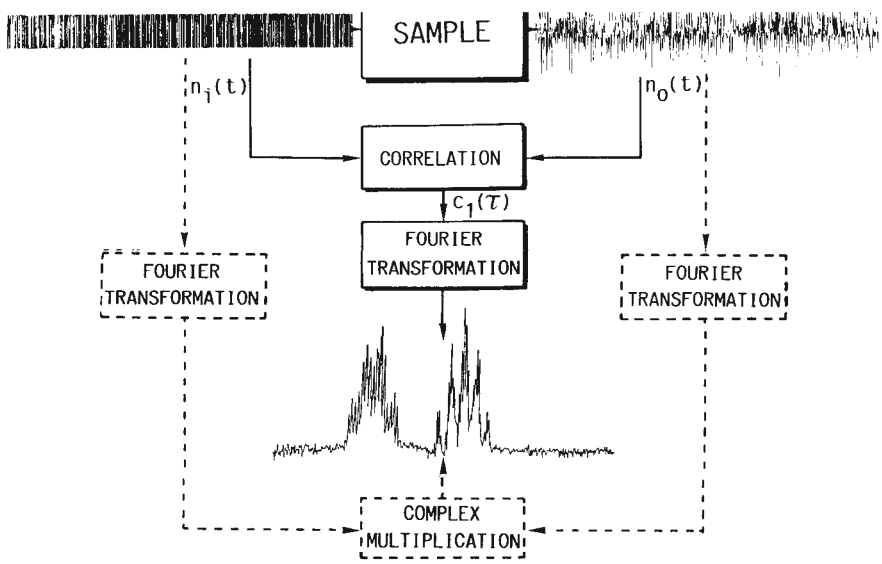

Figure 2. Schematic representation of stochastic resonance by the example of 56.4 MHz fluorine resonance of 2,4-difluorotoluene (33). Excitation with a binary pseudo-random sequence $n_i(t)$ of length 1023 generates the response $n_r(t)$. Cross-correlation of the two signals produces $c_1(\tau)$ which, after Fourier transformation, delivers the shown spectrum. An alternative **procedure**, that has actually been used in this case, computes the individual Fourier transforms of $n_r(t)$ and $n_o(t)$ and multiplies the complex conjugate $\mathcal{F}\{n_i(t)\}^*$ with $\mathcal{F}\{n_o(t)\}$ to obtain the same spectrum.

orine resonance of 2,4-difluorotoluene. A binary pseudo-random sequence of length 1023 with a maximal white spectrum is used for excitation. Its advantages are the predictable spectral properties and the constant rf power. The low peak power puts less stringent requirements on the electronic equipment. Disadvantages concern the simultaneous irradiation and detection that can lead to line broadening effects which are absent in pulse Fourier transform spectroscopy where perturbation and detection are separated in time. A further disadvantage, when using real random noise, is the probabilistic nature of the response that requires extensive averaging to obtain a stable mean value. Higher order correlation functions, such as

$$c_3(\tau_1, \tau_2, \tau_3) = \overline{n_o(t)\, n_i(t-\tau_1)\, n_i(t-\tau_2)\, n_i(t-\tau_3)}, \qquad [4]$$

allow also the characterization of nonlinear transfer properties of the investigated system (26). This has been exploited extensively by Blümich and Ziessow for NMR measurements (34, 35).

A third approach, rapid scan spectroscopy, initially proposed by Dadok and Sprecher (36), achieves a virtually simultaneous excitation of all spins by a rapid frequency sweep through the spectrum (37, 38). The resulting spectrum is strongly distorted, but can be corrected mathematically because of the deterministic nature of the distortions. Correction amounts to convolution with the signal of a single resonance measured under identical conditions or simulated on a computer. An example is given in Fig. 3. It is interesting to note the similarity of a rapid scan spectrum with a FID except for the successively increasing oscillation frequency.

Finally, by computer synthesis, it is possible to compute an excitation function with a virtually arbitrary excitation profile. This has originally been utilized for decoupling purposes by Tomlinson and Hill (39) but is also the

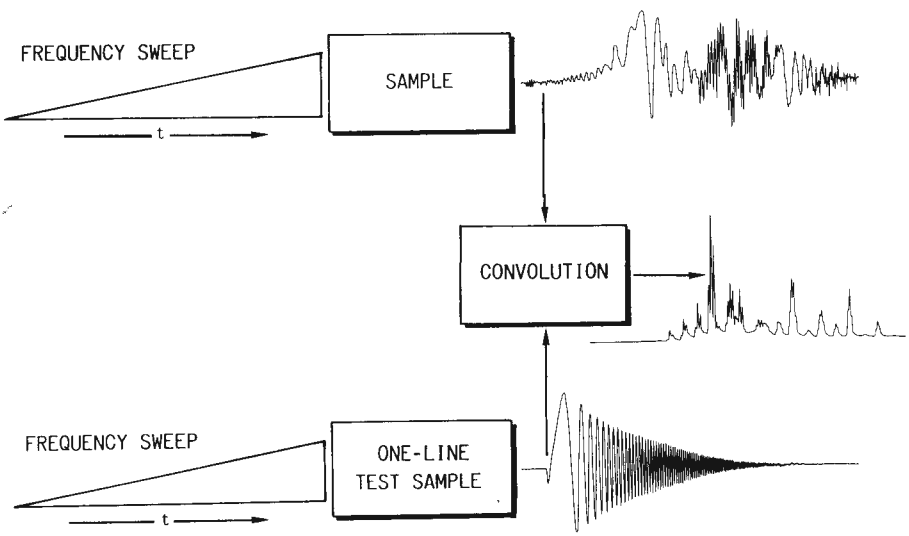

Figure 3. Schematic representation of rapid scan spectroscopy. The strongly distorted sample spectrum obtained by a rapid frequency sweep can be corrected by convolution with the equally sweep-distorted spectrum of a one-line test sample.

basis for composite pulse excitation schemes that have proved to be very powerful (40,41).

Among the broadband excitation techniques, pulse excitation is the only one that allows for a rigorous analytical treatment irrespective of the complexity of the spin system. It does not lead to any method-inflicted line broadening as in stochastic resonance nor to correction-resistant signal distortions as in rapid scan spectroscopy of coupled spin systems (38). Pulse Fourier transform spectroscopy is conceptually and experimentally simple and, last but not least, it can easily be expanded and adapted to virtually all conceivable experimental situations. Relaxation measurements, for example, require just a modified relaxation-sensitive preparation sequence, such as a π—$\pi/2$ pulse pair for T_1 measurements (42) and a $\pi/2$—π pulse pair for T_2 measurements (43). Also the extension to chemical exchange studies using the saturation transfer experiment of Forsén and Hoffman (44) is easily possible.

It should be mentioned at this point that pulsed NMR experiments were suggested already by Felix Bloch in his famous 1946 paper (6), and the first time-domain magnetic resonance experiments have been performed 1949 by H.C. Torrey (45) and, in particular, by Erwin L. Hahn (46-48) who may be regarded as the true father of pulse spectroscopy. He invented the spin echo experiment (46) and devised extremely important and conceptually beautiful solid state experiments (49, 50).

Pulse Fourier transform spectroscopy has not only revolutionized high resolution liquid state NMR spectroscopy, but it has unified NMR methodology across all fields, from solid state resonance, through relaxation measurements, to high resolution NMR, with numerous spill-overs also into other fields such as ion cyclotron resonance (51), microwave spectroscopy (52), and electron paramagnetic resonance (53). In the present context, it provided also the germ for the development of multidimensional NMR spectroscopy.

TWO-DIMENSIONAL FOURIER TRANSFORM SPECTROSCOPY

As long as purely spectroscopic measurements are made, determining the eigenfrequencies or normal modes of a system, one-dimensional spectroscopy is fully adequate. In NMR, this applies to the measurement of the chemical shifts that characterize the local chemical environment of the different nuclei. However, no information can be obtained in this manner on the spatial and topological relations between the observed nuclei.

There are two important pair interactions in nuclear spin systems, the scalar through-bond electron-mediated spin-spin interaction, the so-called J coupling, and the through-space magnetic dipolar interaction. They are illustrated in Fig. 4. The J coupling is represented by the scalar term $\mathcal{H}_{kl} = 2\pi J_{kl}\, \mathbf{I}_k\, I$, in the spin Hamiltonian. It is responsible for the multiplet splittings in high resolution liquid-state spectra. Under suitable conditions, it can lead to an oscillatory transfer of spin order between the two spins I_k

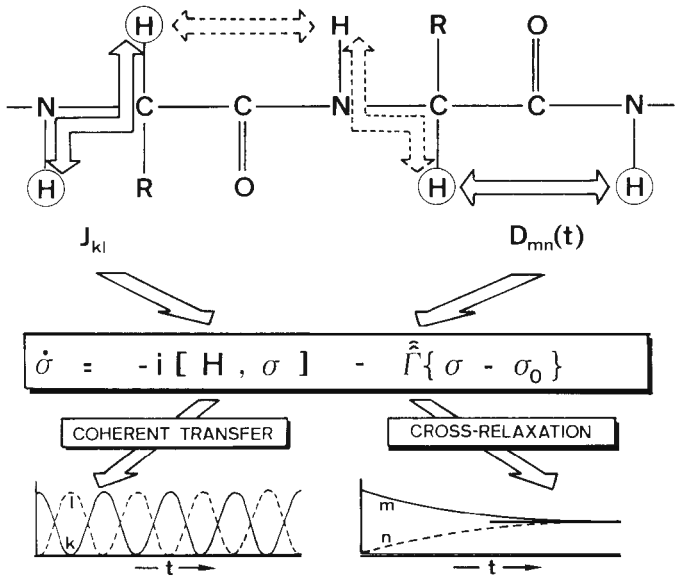

Figure 4. The two pair interactions relevant in NMR. The through-bond scalar J_{kl} coupling contributes to the Hamiltonian and leads to a coherent transfer of spin order between spins I_k and I_l. The time-modulated through-space dipolar interaction $D_{mn}(t)$ causes multiexponential cross relaxation between spins I_m and I_n. The two interactions allow a sequential assignment of the resonances of neighboring spins in the shown peptide fragment and the determination of geometric parameters. The three-bond J coupling is a measure for the dihedral angle about the central bond. The dipolar interaction allows the measurement of internuclear distances.

and I_1. The magnetic dipolar interaction D_{mn}, on the other hand, is represented by a traceless tensor of second rank. Its average in isotropic solution is zero and it can lead to a line splitting only in anisotropic media. However, its time modulation causes also in isotropic solution relaxation processes that are responsible for a multiexponential recovery towards thermal equilibrium among spins after a perturbation. Knowledge of these interactions allows one to deduce geometric information on molecular structure in solution (54, 55) and atomic arrangements in solids. In the optimum case, a complete 5-dimensional structure of a molecule can be deduced (56).

Although these interactions affect 1D spectra, special techniques are needed for their measurement. In the linear response approximation, it is, by first principle, impossible to distinguish between two independent resonances and a doublet caused by a spin-spin interaction. Experiments to explore the nonlinear response properties of nuclear spin systems have been known since the fifties. Saturation studies using strong rf fields yield multiple quantum transitions that contain connectivity information through the simultaneous excitation of several spins belonging to the same coupled spin system (57). Particularly fruitful were double and triple resonance experiments where two or three rf fields are applied simultaneously, resulting in decoupling and spin tickling effects (58-60).

The early multiple resonance experiments have in the meantime been replaced by multi-dimensional experiments. Pair interactions among spins are most conveniently represented in terms of a correlation diagram as shown in Fig. 5. This suggests the recording of a "two-dimensional spectrum" that establishes such a correlation map of the corresponding spectral features. The most straight forward approach may be a systematic double-resonance experiment whose result can be represented as an amplitude $S(\omega_1, \omega_2)$ depending on the frequencies ω_1 and ω_2 of two applied rf fields (8, 58).

A new approach to measure two-dimensional (2D) spectra has been proposed by Jean Jeener at an Ampere Summer School in Basko Polje, Yugoslavia, 1971 (61). He suggested a 2D Fourier transform experiment consisting of two $\pi/2$ pulses with a variable time t_1 between the pulses and the time variable t_2 measuring the time elapsed after the second pulse as shown in Fig. 6 that expands the principles of Fig. 1. Measuring the response $s(t_1, t_2)$ of the two-pulse sequence and Fourier-transformation with respect to both time variables produces a two-dimensional spectrum $S(\omega_1, \omega_2)$ of the desired form (62, 63).

This two-pulse experiment by Jean Jeener is the forefather of a whole class of 2D experiments (8,63) that can also easily be expanded to multi-dimensional spectroscopy. Each 2D experiment, as shown in Figs. 6 and 7, starts with a preparation pulse sequence p which excites coherences, i.e. coherent superpositions represented by the density operator $\sigma(O)$, that are allowed to precess for an evolution time t_1 under the evolution superoperator $\hat{\hat{E}}(t_1)$. During this period, the coherences are so-to-say frequency-labelled. A following mixing sequence $\hat{\hat{R}}$ performs a controlled transfer of coherence to different nuclear spin transitions that evolve then during the detection period as a function of t_2 under the evolution superoperator $\hat{E}(t_2)$.

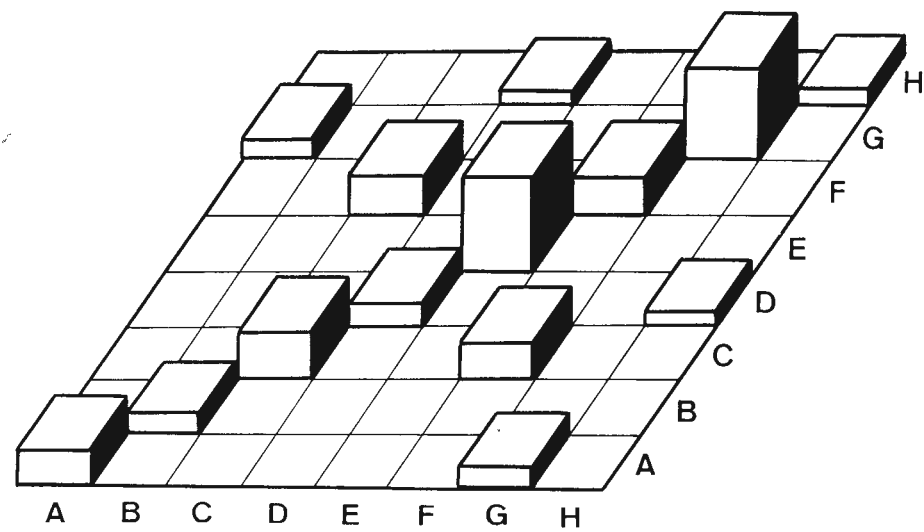

Figure 5. Schematic correlation diagram for the representation of internuclear pair interactions.

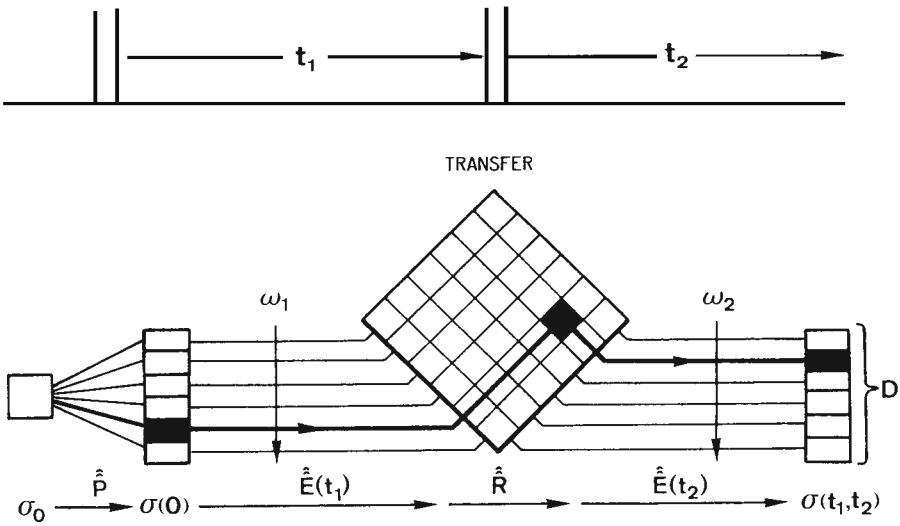

Figure 6. Schematic representation of a 2D experiment, here with a simple two-pulse sequence. The first pulse excites coherences that precess during t_1 and are transfered by the second pulse to different transitions where the coherences continue to precess with a new frequency. The 2D spectrum obtained by a 2D Fourier transformation of $<D>(t_1, t_2)$ provides a visual representation of the transfer matrix R.

Detection is performed with the detection operator D in analogy to Fig.1, leading to the expression

$$<D>(t_1, t_2) = \mathrm{Tr}\{ D\hat{\hat{E}}(t_2)\hat{\hat{R}}\hat{\hat{E}}(t_1)\hat{\hat{P}}\sigma_0\}. \qquad [5]$$

It is not sufficient to perform a single two-pulse experiment. To obtain the necessary data $<D>(t_1, t_2)$ to compute a 2D spectrum $S(\omega_1, \omega_2)$, it is required to systematically vary t_1 in a series of experiments and to assemble a 2D data matrix that is then Fourier transformed in two dimensions as is indicated schematically in Fig. 7. The resulting 2D spectrum correlates the precession frequencies during the evolution period with the precession frequencies during the detection period. It represents a vivid and easily interpretable representation of the mixing process. Diagonal and cross peaks are measures for the elements of the transfer matrix of the mixing pulse sequence in Fig. 6.

Among the numerous transfer processes that can be represented in this manner, the most important ones are (8)

(i) the scalar J coupling, leading to "2D correlation spectroscopy", abbreviated COSY,

(ii) internuclear cross relaxation, leading to "2D nuclear Overhauser effect spectroscopy", abbreviated NOESY, and

(iii) chemical exchange, leading to "2D exchange spectroscopy", abbreviated EXSY.

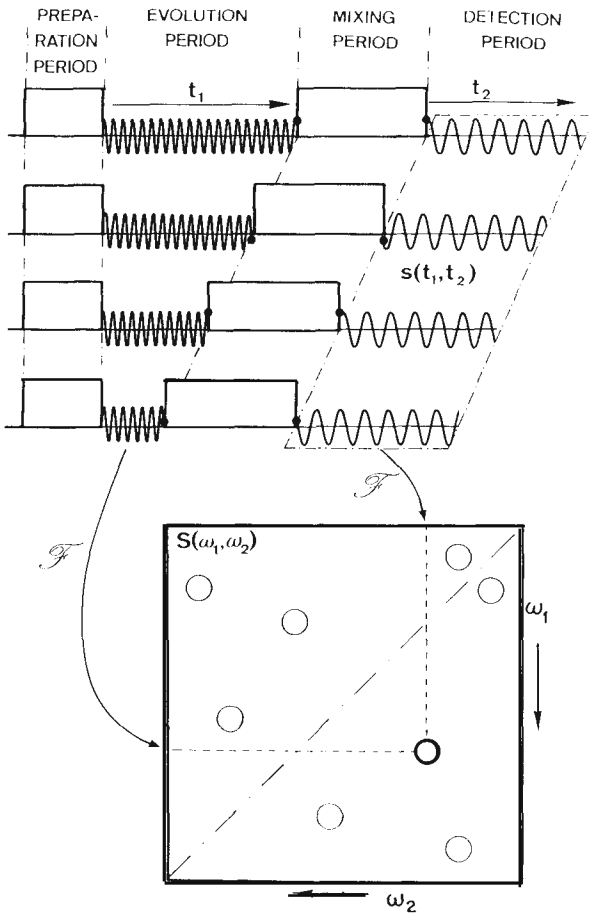

Figure 7. General 2D experiment consisting of a preparation, an evolution, a mixing, and a detection period. The duration t, of the evolution period is varied systematically from experiment to experiment. The resulting signal $s(t_1, t_2)_\alpha < D > (t_1, t_2)$ is Fourier-transformed in two dimensions to produce the 2D spectrum $S(\omega_1,\omega_2)$.

The COSY transfer (i), which proceeds through J coupling, is truly a quantum mechanical effect that does not find a satisfactory classical explanation. By means of a single $(\pi/2)_x$ rf mixing pulse, as in Fig. 6, it is possible to transfer coherence of spin k, anti-phase with respect to spin 1 and represented in the density operator by the operator term $2I_{ky}I_{1z}$ into coherence of spin 1, anti-phase with respect to spin k, represented by $-2I_{kz}I_{1y}$:

$$2I_{ky}I_{1z} \xrightarrow{(\pi/2)_x} -2I_{kz}I_{1y} \qquad [6]$$

whereby each factor of the above product spin operator can be considered to be rotated by $\pi/2$ about the x axis. Anti-phase coherence of the type $2I_{ky}I_z$ is only formed during the evolution period when there is a direct spin-spin coupling between the spins I_k and I_l:

$$I_{kx} \xrightarrow{2\pi J_{kl}I_{kz}I_{lz}t_1} I_{kx}\cos(\pi J_{kl}t_1) + 2I_{ky}I_{lz}\sin(\pi J_{kl}t_1). \qquad [7]$$

This implies that in a two-dimensional correlation spectrum there are cross peaks only between directly coupled spins (as long as the weak coupling approximation holds). It is also obvious from Eq.[7] that there is no net coherence transfer, e.g. $I_{kx} \rightarrow I_{lx}$, and the cross-peak integral must disappear, in other words, there is an equal number of cross-peak multiplet lines with positive and negative intensity.

A COSY spectrum, such as the one shown in Fig. 8 for the cyclic decapeptide antamanide (I)

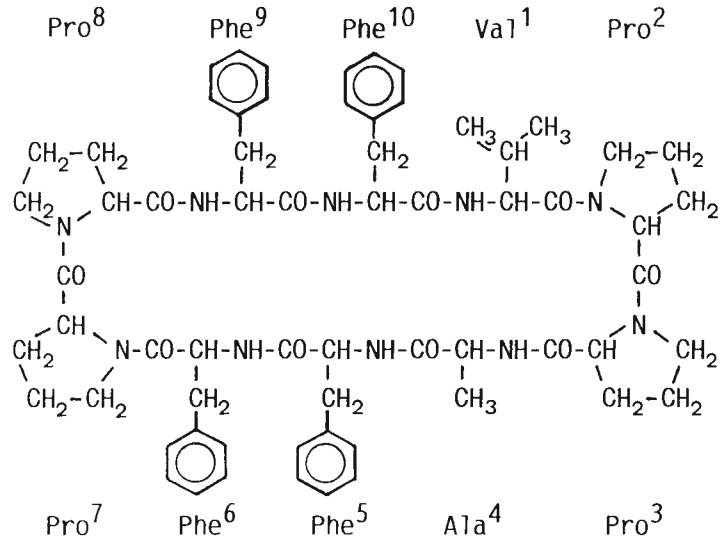

(I)

can be used to find pairs of spins belonging to the same coupling network of an amino acid residue in the molecule. All strong cross peaks arise from two-bond and three-bond couplings that allow, first of all, the assignment of the pairs of NH and CαH backbone protons, as indicated by C in Fig. 9 for the six amino acid residues with NH protons. In addition, it is also possible to assign the side-chain protons.

The transfers (ii) and (iii) of NOESY and EXSY experiments involve incoherent, dissipative processes that drive the system back to equilibrium after an initial perturbation in an exponential or multiexponential manner. They require an extended mixing time during which the random processes are given a chance to occur. Both processes can be investigated with the same three-pulse scheme shown in Fig. 10b (8, 64-67). The mixing period is bracketed by two $\pi/2$ pulses that transform coherence into static spin order and back into coherence. The exchange processes transfer the spin order between different spins or between different chemical species, respectively. This type of transfer can be understood based on classical kinetic models. The resulting 2D spectrum represents a kinetic matrix with cross-peak intensities proportional to the exchange-rate constants of pseudo first order reactions

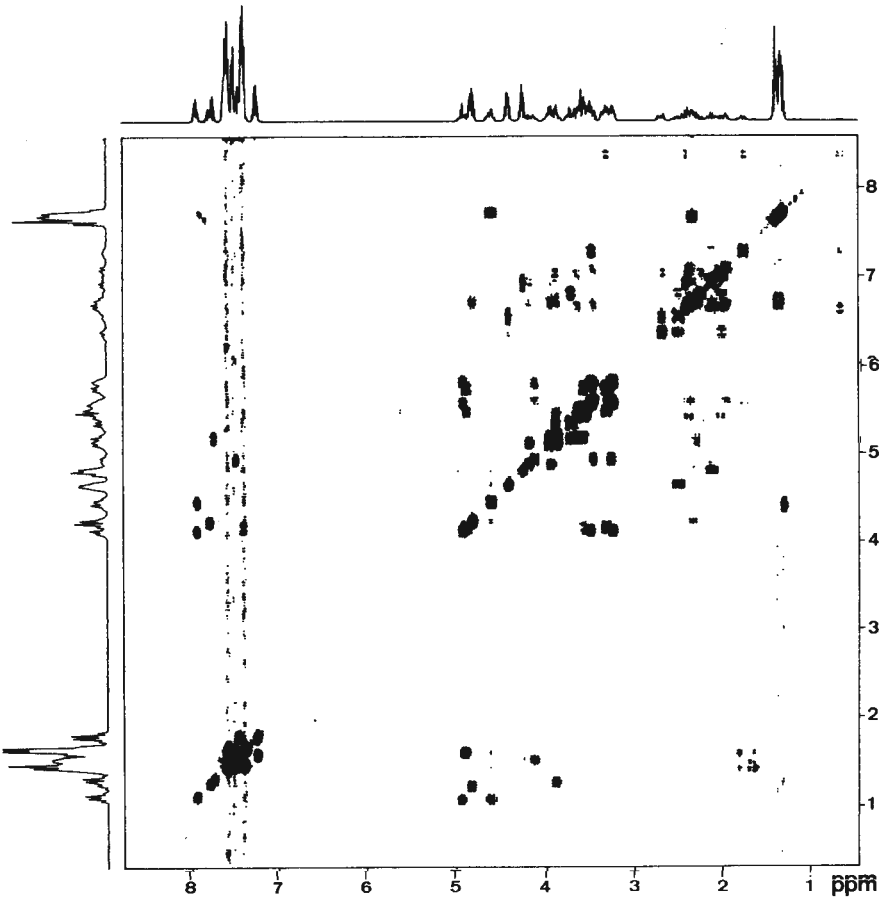

Figure 8. **Phase-sensitive 400 MHz proton resonance COSY spectrum of antamanide in chloroform solution (at 250 K) in a contour-line representation.** Positive and negative contours are not distinguished. The spectrum has been recorded by Dr. Martin Blackledge.

For the NOESY transfer, the exchange-rate constants are given by the cross-relaxation rate constants, that are due to magnetic dipolar interaction, and are proportional to $1/r_{kl}^6$ for nuclear pairs I_k and I_l in addition to a dependence on the correlation time τ_c of the molecular tumbling in solution. The distance dependence can be used to measure relative or, if τ_c is known, absolute distances in molecules. In the course of the assignment process, the NOESY cross peaks allow an identification of spatially neighboring protons in a molecule, important for protons that belong to adjacent amino acid residues in peptides. A NOESY spectrum of antamanide is given in Fig. 11. The cross peaks between sequential backbone protons of adjacent amino acid residues, contained in Fig. 11, are marked in Fig. 9 by N. It is seen that, together with the J-cross peaks from the COSY spectrum of Fig. 8, two unbroken chains of connectivities are found that can be used for the identification of the backbone protons. The two chains are disjoint due to the absence of NH protons in the four proline residues. The general assignment procedure of proton resonance frequencies based on COSY

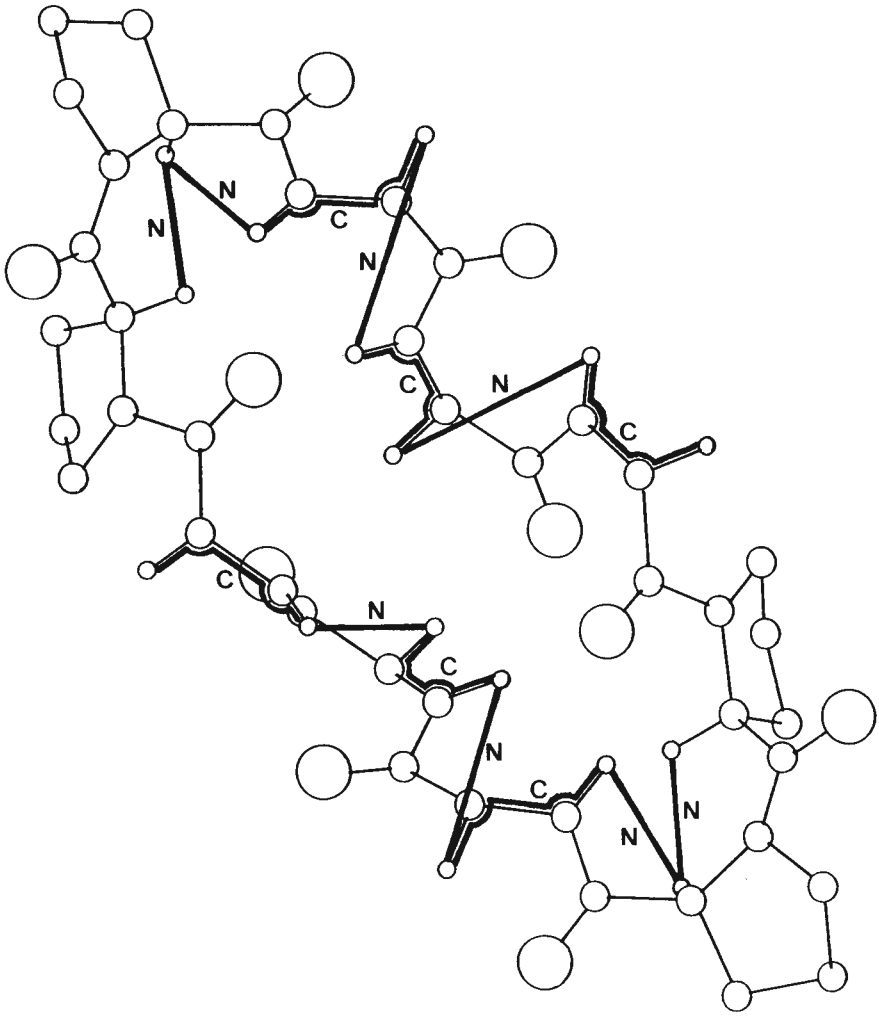

Figure 9. Assignment of backbone protons in antamanide by the combination of COSY (C) and NOESY (N) cross peaks. The missing NH protons in the four proline residues break the chain of sequential C,N connectivities.

and NOESY spectra has been established by Wüthrich and his research group (56).

Based on a complete or partial set of assigned resonances, it is then possible to deduce molecular structural information. Each NOESY cross-peak intensity delivers an internuclear distance that can be used in a manual or computerized process to construct a molecular model that is compatible with the experimental data. In this process it is also possible to employ scalar coupling constants extracted from COSY-type spectra (most conveniently from E.COSY spectra, as mentioned later). According to the Karplus-relations (54), there is an accurate relation between vicinal coupling constants and dihedral angles. Ingenious computer procedures to determine molecular structures based on NMR data have, for the first time, been

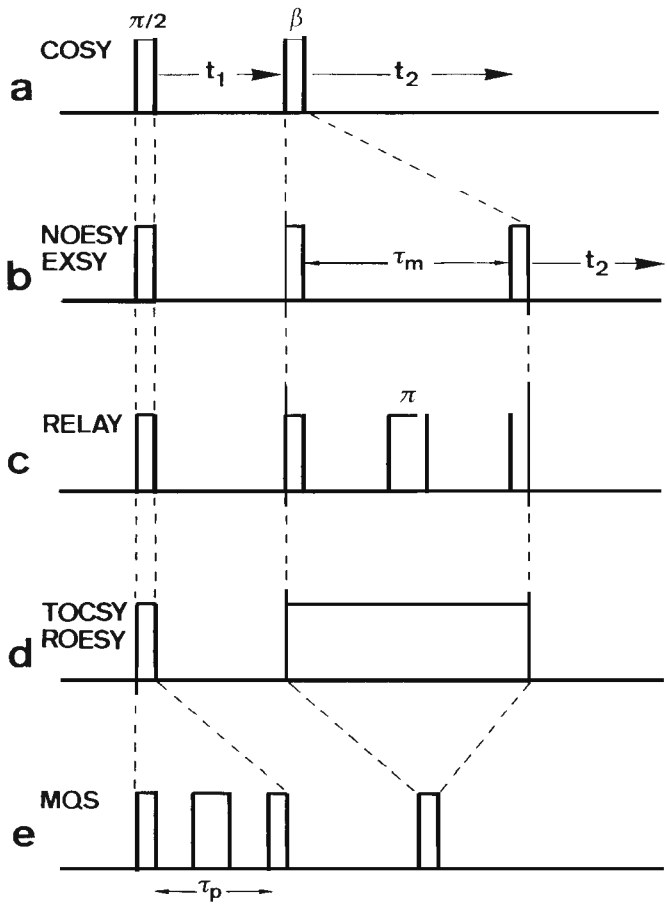

Figure 10. Some of the most useful homonuclear 2D experiments: (a) COSY, (b) NOESY or EXSY, (c) relayed COSY, (d) TOCSY or ROESY in the rotating coordinate system, (e) multiple quantum spectroscopy.

developed by Kurt Wüthrich and his research team and tested on a large number of small to medium-size proteins (56, 68-71). At present, mainly two computer algorithms for the structure determination are in use, the distance geometry algorithm (72, 73) and modifications of it and the restrained molecular dynamics algorithm (74, 75), again with many variations. The structural problem in antamanide will be discussed later, as it involves intramolecular dynamic processes that complicate the situation.

Cross peaks in a NOESY-type exchange spectrum can also originate from process (iii), i.e. from chemical exchange, and the three-pulse experiment of Fig. 10b is indeed very suited to investigate chemical exchange networks (64, 65, 76). A distinction of the two types of peaks is not possible by inspection of a single 2D spectrum. However, variable temperature studies are often conclusive. At sufficiently low temperature where chemical exchange becomes slow, only NOESY cross peaks should remain. Another way of distinction are rotating frame experiments as mentioned in the next section.

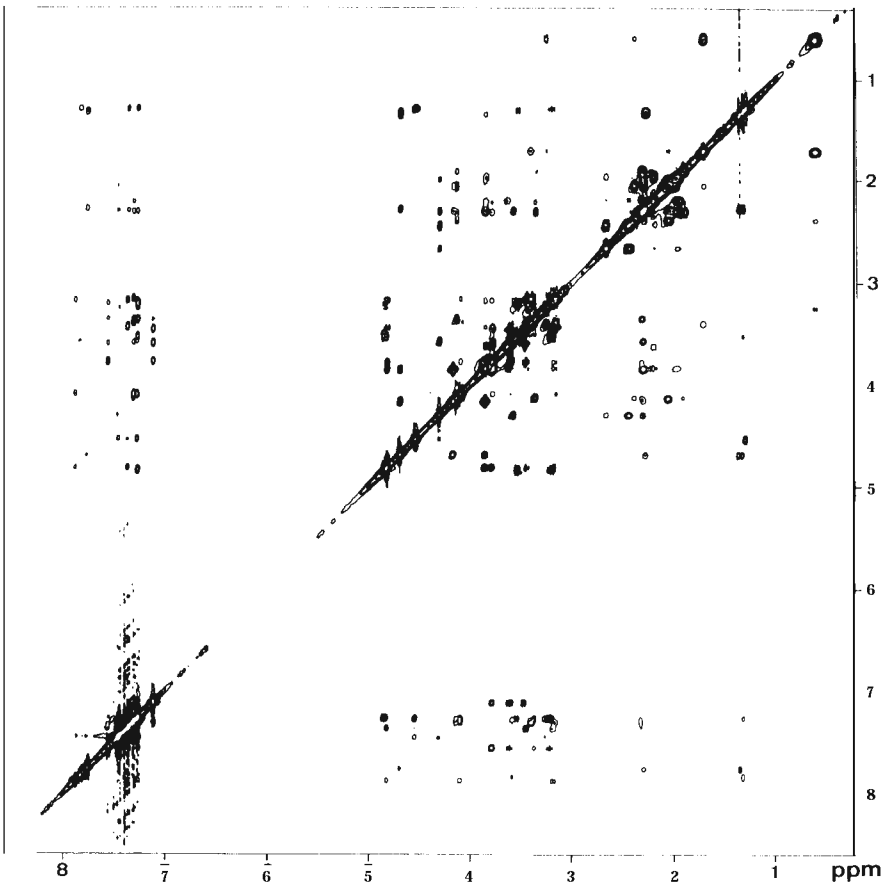

Figure 11. 400 MHz proton resonance NOESY spectrum of antamanide in chloroform (at 250K) in a contour-line representation. The spectrum has been recorded by Dr. Martin Blackledge.

A typical ^{13}C chemical exchange spectrum of a mixture of cis-decalin and trans-decalin is given in Fig. 12. The spectrum demonstrates the well known conformational stability of trans-decalin whereas four pairs of carbon spins of cis-decalin are involved in a conformational exchange process, giving rise to two pairs of cross peaks (76).

MODIFIED TWO-DIMENSIONAL FOURIER EXPERIMENTS

Starting from the two prototype 2D Fourier experiments, an enormous number of modified, expanded, and improved experiments has been suggested. Many of them have found a place in the routine arsenal of the NMR spectroscopist. A first class of experiments, as visualized in Fig. 13, causes extended correlation through two or more transfer steps: Relayed correlation experiments involve two-step correlation and total correlation spectroscopy (TOCSY) achieves multiple step correlation. The latter experiment leads to the important class of rotating frame experiments, including rotating frame Overhauser effect spectroscopy (ROESY) an alternative to

NOESY. Finally, also multiple quantum spectroscopy allows one to investigate connectivity in spin systems. A second class of experiments attempts the simplification of spectra by exclusive correlation (E.COSY), multiple quantum filtering, and spin-topology filtration.

Relayed Correlation

In a standard COSY experiment, coherence is transfered exclusively between two directly coupled spins by means of a single mixing pulse. By a

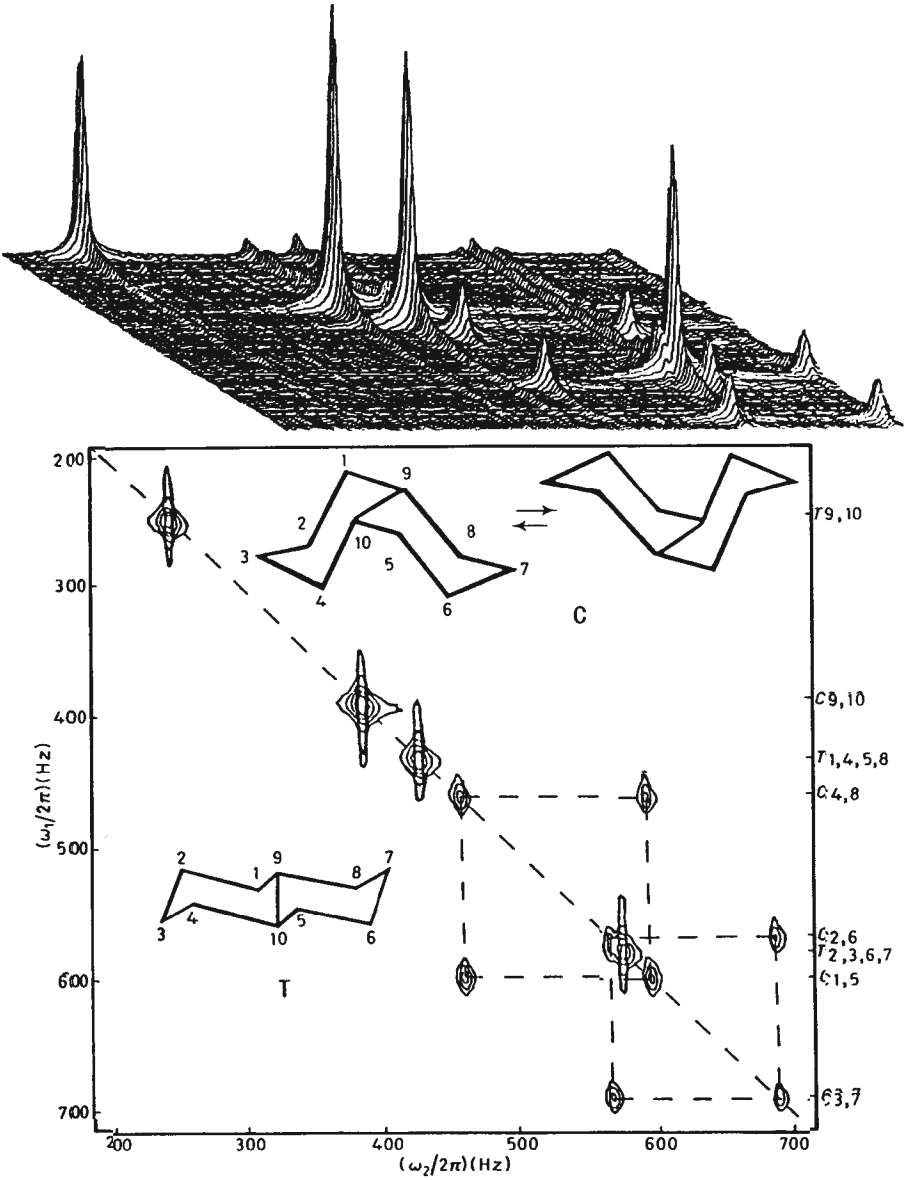

Figure 12. 2D ^{13}C chemical exchange spectrum (EXSY) of a mixture of cis- and trans-decalin recorded at 22.5 MHz and 241K (76). A stacked plot and a contour representation are given with the assignment of the peaks.

sequence of two $\pi/2$ pulses, as in Fig. 10c, it is possible to effect a transfer across two sequential couplings from spin I_k to spin I_l through the relay spin I_r (77,78)

$$I_{kz} \xrightarrow{(\pi/2)I_{ky}} I_{kx} \xrightarrow{2\pi J_{kr} I_{kz} I_{rz} t_1} 2I_{ky}I_{rz} \xrightarrow{(\pi/2)(I_{kx}+I_{rx})}$$

$$-2I_{kz}I_{ry} \xrightarrow{2\pi J_{kr} I_{kz} I_{rz} \tau_m + 2\pi J_{rl} I_{rz} I_{lz} \tau_m} 2I_{ry}I_{lz} \xrightarrow{(\pi/2)(I_{rx}+I_{lx})} -2I_{rz}I_{ly} \quad [8]$$

(assuming $J_{kr}t_1 = J_{kr}\tau_m = J_{rl}\tau_m = 1/2$). During the extended mixing period τ_m, it is thus necessary to refocus the anti-phase character of the I_r spin coherences with respect to spin I_k and create anti-phase character with respect to spin I_l to allow for a second transfer by the second mixing pulse. Relayed correlation is useful whenever the resonance of the relay spin I_r cannot unambiguously be identified. With a relay experiment it is then nevertheless possible to assign spins I_k and I_l to the same coupling network (e.g. belonging to the same amino acid residue in a polypeptide chain). It is

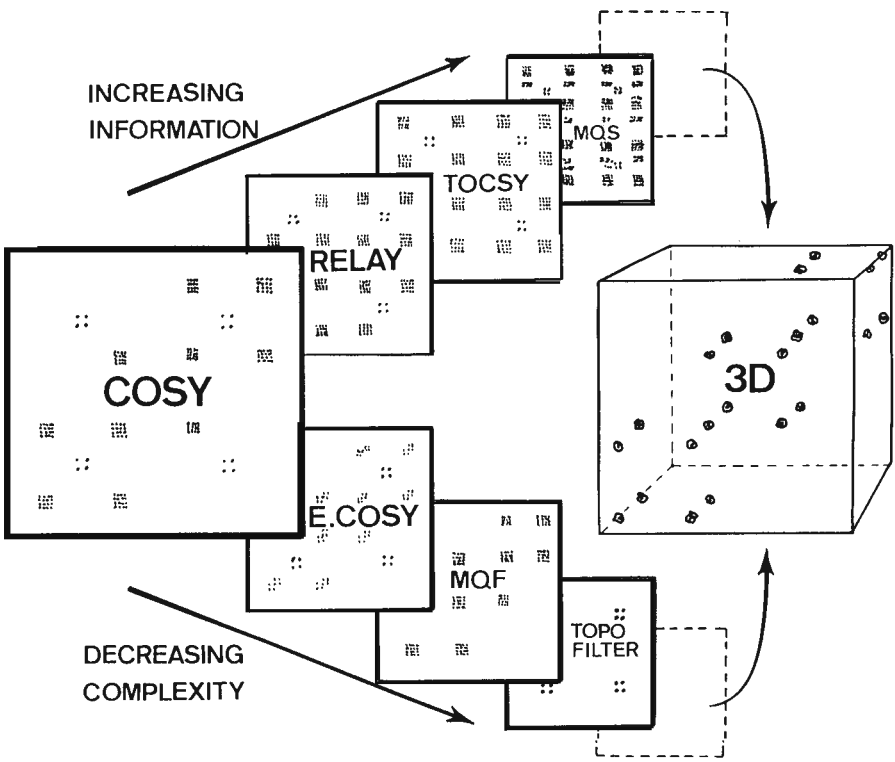

Figure 13. Extensions of the standard COSY experiment. Relayed correlation, total correlation spectroscopy (TOCSY), and multiple quantum spectroscopy (MQS) increase the information content, while exclusive correlation (E.COSY), multiple quantum filtering (MQF), and spin topology filtration reduce the complexity. Both avenues can lead to three-dimensional spectroscopy.

usually of advantage to refocus the effects of the chemical shift precession during the mixing period by incorporating a central π pulse as in Fig.

Relayed coherence transfer is demonstrated by 300 MHz proton resonance spectra of the linear nonapeptide buserilin, pyro-Glu-His-Trp-Ser-Tyr-D-Ser-Leu-Arg-Pro-$NHCH_2CH_3$. Figure 14a shows a (double-quantum filtered) COSY spectrum and Fig. 14b the corresponding relayed COSY spectrum (79). In both spectra, the resonance connectivities for the residue leucine are marked. It is evident that in the COSY spectrum only nearest neighbor protons are connected by cross peaks: NH—$C_\alpha H$, $C_\alpha H$—$C_\beta H^{1,2}$, $C_\beta H^{1,2}$—$C_\gamma H$, and $C_\gamma H$—$(C_\delta H_3)^{1,2}$. On the other hand in the relayed COSY spectrum, also the next nearest neighbors NH—$C_\beta H^{1,2}$ and $C_\beta H^{1,2}$—$(C_\delta H_3)^{1,2}$ are connected. The third pair of relayed cross peaks $C_\alpha H$—$C_\gamma H$ is weak due to the high multiplicity of the $C_\gamma H$ resonance and not visible in the contour representation of Fig. 14b. Similar relayed cross peaks can be found for the other amino acid residues.

Rotating Frame Experiments

By means of an extended mixing pulse sequence, transfer of coherence over an arbitrary number of steps is in principle possible. In particular, continuous wave irradiation leads to the mixing of all eigenmodes of a spin system and correspondingly to transfers of coherence between all of them. This is exploited in total correlation spectroscopy (TOCSY) with the sequence of Fig. 10d. All spins belonging to the same J-coupling network can be identified with TOCSY (80,81). The accurate matching of the precession frequencies of the various spins in the presence of a radio frequency field is crucial to enable an efficient transfer of coherence. Either very strong radio frequency fields or specially designed pulse sequences are needed for this purpose (81). Coherence transfer is possible when the effective average magnetic field strengths B_k^{eff} in the rotating frame are equal within a J-coupling constant, $|\gamma(B_k^{eff} - B_l^{eff})| < |2\pi J_{kl}|$, corresponding to a strong coupling case in the rotating frame.

The TOCSY experiment is of interest for assigning proton resonances to individual amino acid residues in a protein. Of particular value is that its transfer rate is enhanced by a factor 2 in comparison to COSY or relayed transfer experiments in the laboratory frame (80). Another property is that, due to the presence of a radio-frequency field, in-phase coherence transfer of the type

$$I_{kx} \xrightarrow{2\pi J_{kl}\, \mathbf{I}_k\, \mathbf{I}_l \tau_m} I_{lx} \qquad [9]$$

is possible, leading to in-phase cross-peak multiplet structures.

A TOCSY spectrum of buserilin is included in Fig. 14c for comparison with the relayed and standard COSY spectra given. Here also three-step transfers $C_\alpha H$—$(C_\delta H_3)^{1,2}$ and even four-step transfers NH—$(C_\delta H_3)^{1,2}$ are visible. Again, some expected cross peaks involving $C_\gamma H$ are missing because of the extensive multiplet structure of $C_\gamma H$.

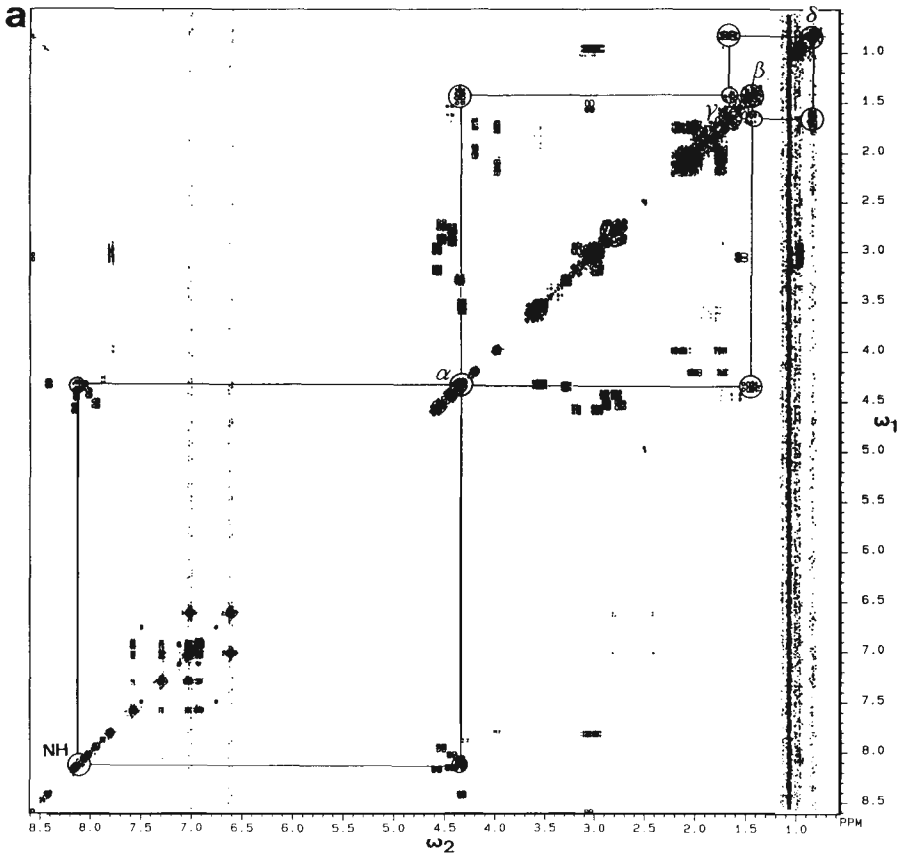

Figure 14. 300 MHz correlation spectra of the nonapeptide buserilin dissolved in dimethyl sulfoxide. Phase-sensitive plots with equal representation of positive and negative contours are shown. The resonance connectivities are indicated for leucine (79). (a) Double quantum-filtered COSY spectrum using the sequence of Fig. 18. (b) Relayed COSY spectrum using the sequence of Fig. 10c with τ_m = 25 ms. (c) TOCSY spectrum using the sequence of Fig. 10d with τ_m = 112ms and an MLEV-17 pulse sequence applied during τ_m.

The elimination of the chemical shift precession by the rf irradiation leads, in addition to the coherent transfer through the J-coupling network, also to an incoherent transfer of spin order through transverse cross relaxation. The transverse cross-relaxation terms are, in principle, always present. However, strong differential chemical shift precession of spin pairs causes normally a quenching of the transfer in the sense of first order perturbation theory. In the presence of a strong rf field, this quenching is no longer operative and transverse cross relaxation occurs. This is the transfer mechanism of the rotating frame Overhauser effect spectroscopy (ROESY) experiment (82).

ROESY has similar properties as NOESY but differs in the dependence of the cross-relaxation rate constant Γ_{kl} on the correlation time τ_c of the molecular rotational motion that modulates the internuclear dipolar interaction, responsible for cross relaxation:

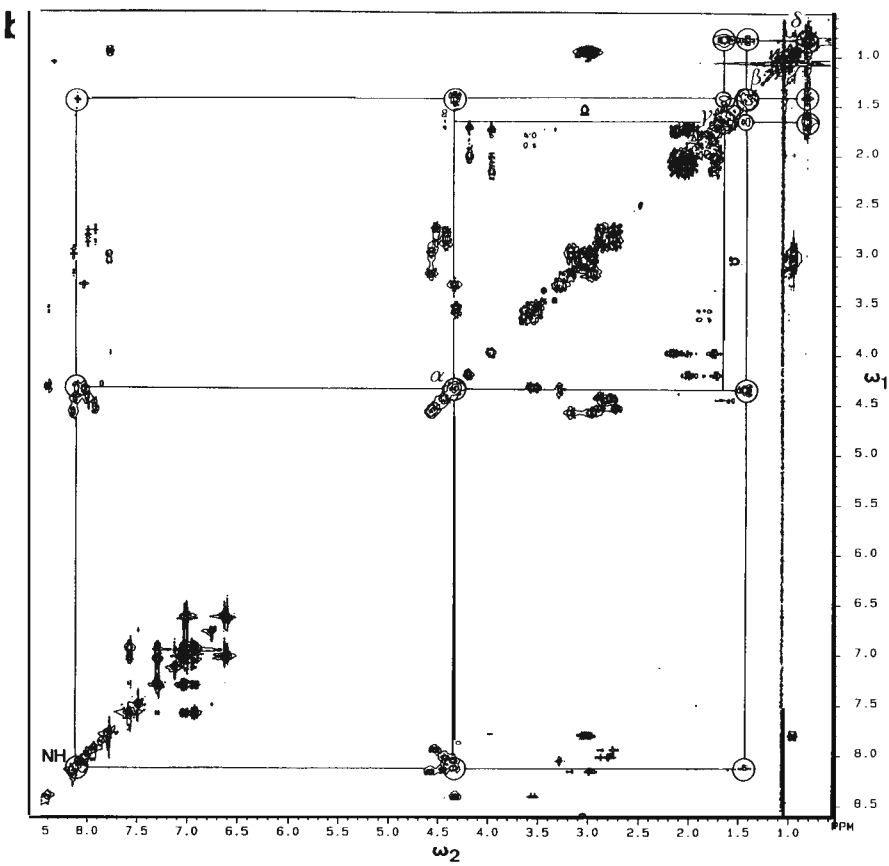

Figure 14 b

$$\Gamma^{NOE}_{kl} = \frac{\gamma^4 \hbar^2}{10\, r_{kl}^6} \left(\frac{\mu_0}{4\pi}\right)^2 \quad \left[-\frac{1}{2} J(0) + 3J(2\omega_0)\right], \qquad [10]$$

$$\Gamma^{ROE}_{kl} = \frac{\gamma^4 \hbar^2}{10\, r_{kl}^6} \left(\frac{\mu_0}{4\pi}\right)^2 \quad \left[J(0) + \frac{3}{2} J(\omega_0)\right], \qquad [11]$$

with the spectral density

$$J(\omega) = 2\tau_c/(1+(\omega\tau_c)^2), \qquad [12]$$

ω_0 is as usual the Larmor frequency of the two nuclei with the internuclear distance r_{kl}. This implies that Γ^{NOE}_{kl} changes sign for an intermediate correlation time $\tau_c = (5/4)^{1/2}/\omega_0$, whereby the cross-relaxation rate constant becomes small in the neighborhood of this condition. Depending on the viscosity of the solvent and the resonance frequency ω_0, this occurs for globular molecules within a range of molecular mass of 500—2000 Dalton. Γ^{ROE}_{kl}, on the other hand, is less sensitive to τ_c and remains positive for any molecular mass. The ROESY experiment is therefore of advantage for molecules of intermediate size.

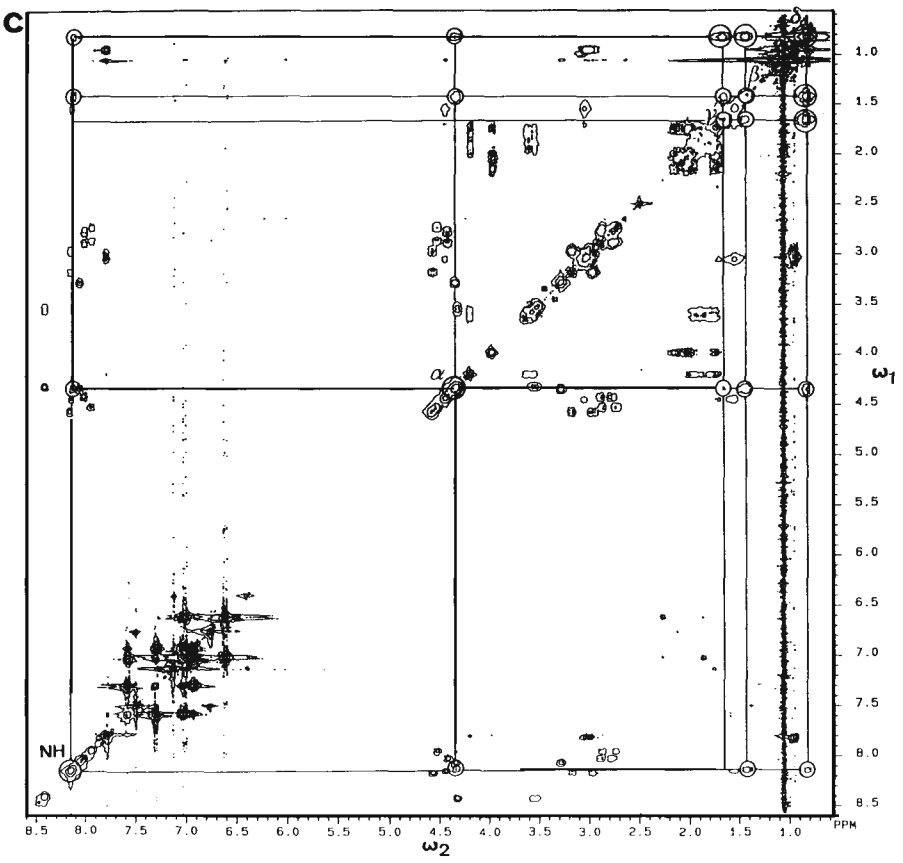

Figure 14 c.

The different sensitivity of NOE and ROE on τ_c allows one, in addition, to deduce information on intramolecular mobility by comparison of the two measurements (83). An advantage of ROESY in comparison to NOESY is the negative cross-peak amplitude for ROESY while the simultaneously occurring chemical exchange cross peaks are positive and allow for an easy distinction unless they overlap.

It should be recognized that in the rotating frame coherence transfer through J couplings and cross relaxation occur simultaneously, TOCSY cross peaks being positive while ROESY cross peaks appear with negative amplitude. This complicates the 2D spectra and calls for separation procedures. The suppression of the coherent transfer through J couplings (TOCSY) is easy as it is just necessary to mismatch the condition $|\gamma(B_k^{eff} - B_l^{eff})| < |2\pi J_{kl}|$, for example by a slight frequency offset in the presence of not too strong rf fields. The cross-relaxation rates are much less sensitive to such a mismatch such that a clean ROESY spectrum results.

To obtain a clean TOCSY spectrum is more demanding as relaxation cannot easily be manipulated. A "clean TOCSY" technique has been proposed by C. Griesinger (84). It relies on a combination of Eqs. [10] and [I I] to cause a vanishing average cross-relaxation rate constant:

$$\bar{\Gamma}_{kl} = p\,\Gamma^{NOE}_{kl} + (1-p)\,\Gamma^{ROE}_{kl} \stackrel{!}{=} 0. \qquad [13]$$

A suitable weight p can be found whenever $\Gamma^{NOE}_{kl} < 0$, i.e. for sufficiently large molecules with $\tau_c > (5/4)^{1/2}/\omega_0$. This requires the magnetization to move on a trajectory that spends a fractional time p along the z axis and a fraction (1 - p) in the transverse plane. For $\tau_c \rightarrow \infty$, one finds p = 2/3 for $\bar{\Gamma}_{kl} = 0$. A suitable pulse sequence, modifying an MLEV-17 spin locking sequence, has been proposed in Ref. 84. Another optimized sequence, called 'clean CITY', has been developed by J. Briand (85). A clean TOCSY spectrum of basic pancreatic trypsin inhibitor (BPTI) using the clean CITY sequence is compared in Fig. 15 with a conventional TOCSY spectrum to demonstrate the efficient suppression of the (negative) ROESY peaks.

Multiple Quantum Spectroscopy

In spectroscopy, in general, only those transitions are directly observable for which the observable operator has matrix elements different from zero, leading to the so-called allowed transitions. In high field magnetic resonance with weak continuous wave perturbation or observing the free induction decay in the absence of rf, the transverse magnetization observable operator $F_x = \sum_k I_{kx}$ has matrix elements only between eigenstates of the Hamiltonian differing in the magnetic quantum number M by ± 1. Thus, single quantum transitions are the allowed transitions, multiple quantum transitions with $|\Delta M| > 1$ being forbidden. Multiple quantum transitions can however be induced by strong continuous wave rf fields that cause a mixing of states (8, 57) or by a sequence of at least two rf pulses (8, 63, 86, 87). Observation is possible again in the presence of a strong rf field (8, 57) or after a further detection pulse (8, 63, 86, 87).

For spin I = 1/2 systems, multiple quantum transitions invariably involve several spins, and multiple quantum spectra contain information on the connectivity of spins within the J-coupling network in analogy to 2D correlation spectra. In particular, the highest order transition allows one to determine the number of coupled spins. Relaxation rate constants of multiple quantum coherences are dependent on the correlation of the random perturbations affecting the involved spins and deliver information on motional processes (88).

A simple instructive example of a 2D double quantum spectrum is given in Fig. 16 to demonstrate the use of multiple quantum transitions for the assignment of resonances (89). Along ω_1, double quantum transitions and along ω_2 single quantum transitions are displayed for the six-spin system of 3-aminopropanol-d_3 ($DOCH_2CH_2CH_2ND_2$). In general, there are three different categories of double quantum transitions:

(I) Double quantum transitions involving two directly coupled spins. They lead to pairs of cross peaks displaced symmetrically from the double quantum diagonal ($\omega_1 = 2\omega_2$) with ω_2 coordinates corresponding to the Larmor frequencies of the two spins (e.g. $\omega_1 = \Omega_A + \Omega_M$, $\Omega_M + \Omega_X$).

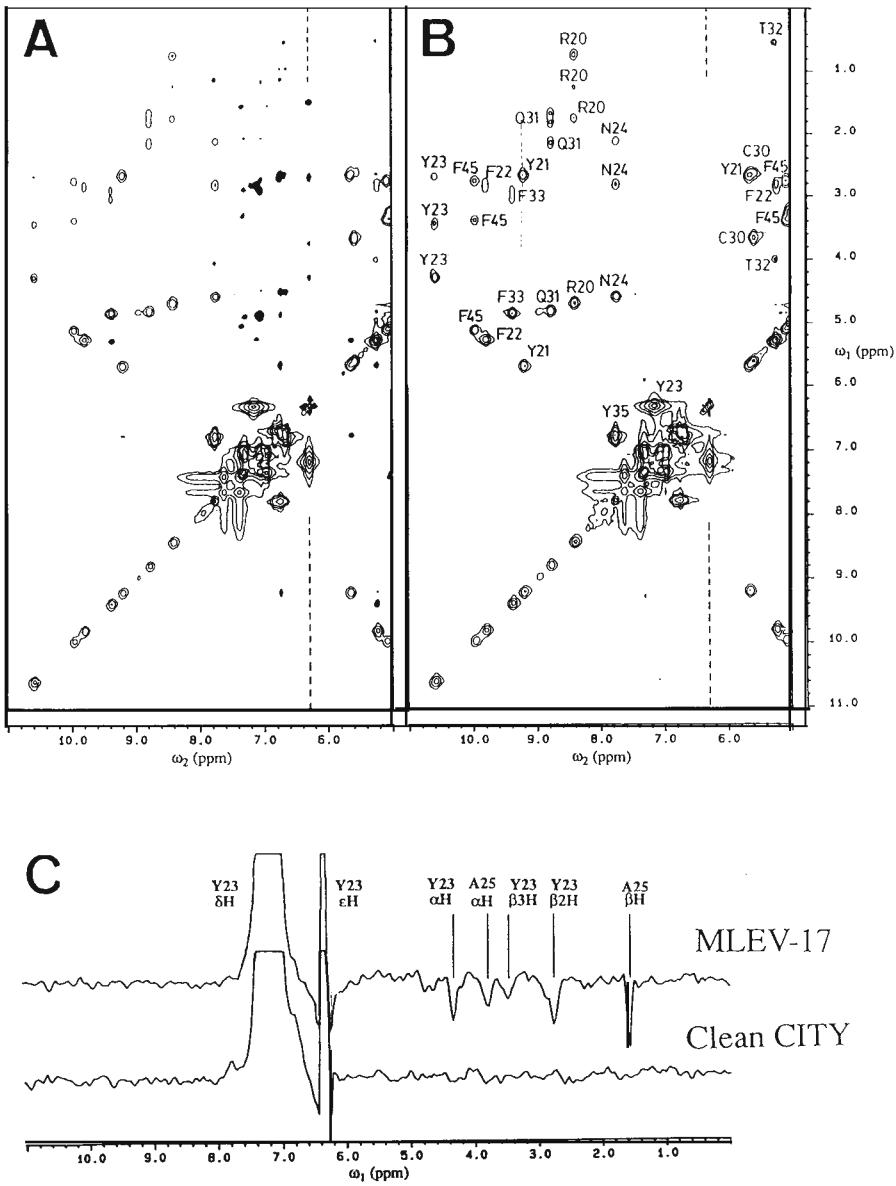

Figure 15. Phase-sensitive 300 MHz ^{1}H TOCSY spectra of 15 mM bovine pancreatic trypsin inhibitor in D_2O recorded with a 69ms mixing time (85). (a) Mixing process with MLEV-17 pulse sequence. Negative peaks are shown by contours filled in black. (b) Mixing process with clean CITY pulse sequence. (c) Cross sections along ω_1 through the Tyr^{23} εH diagonal peak at 6.33ppm in the two spectra (a) and (b) (see broken lines).

(II) Double quantum transition involving two magnetically equivalent spins. They lead to one or more cross peaks at an ω_1 frequency that intersects the double quantum diagonal at the ω_2 frequency corresponding to the common Larmor frequency of the two spins (e.g. $\omega_1 = 2\,\Omega_A, 2\,\Omega_M, 2\,\Omega_X$, although the spins are only within experimental accuracy magnetically equivalent).

(111) Double quantum transitions involving two remotely coupled spins. They lead to single cross peaks at an ω_1 frequency that intersects the double quantum diagonal at ω_2 equal to the mean of the two Larmor frequencies (e.g. $\omega_1 = \Omega_A + \Omega_x$). These cross peaks carry information identical to that in relayed correlation spectra.

For the practical application it is essential that a multiple quantum spectrum never contains a strong diagonal peak array. It should be mentioned that a

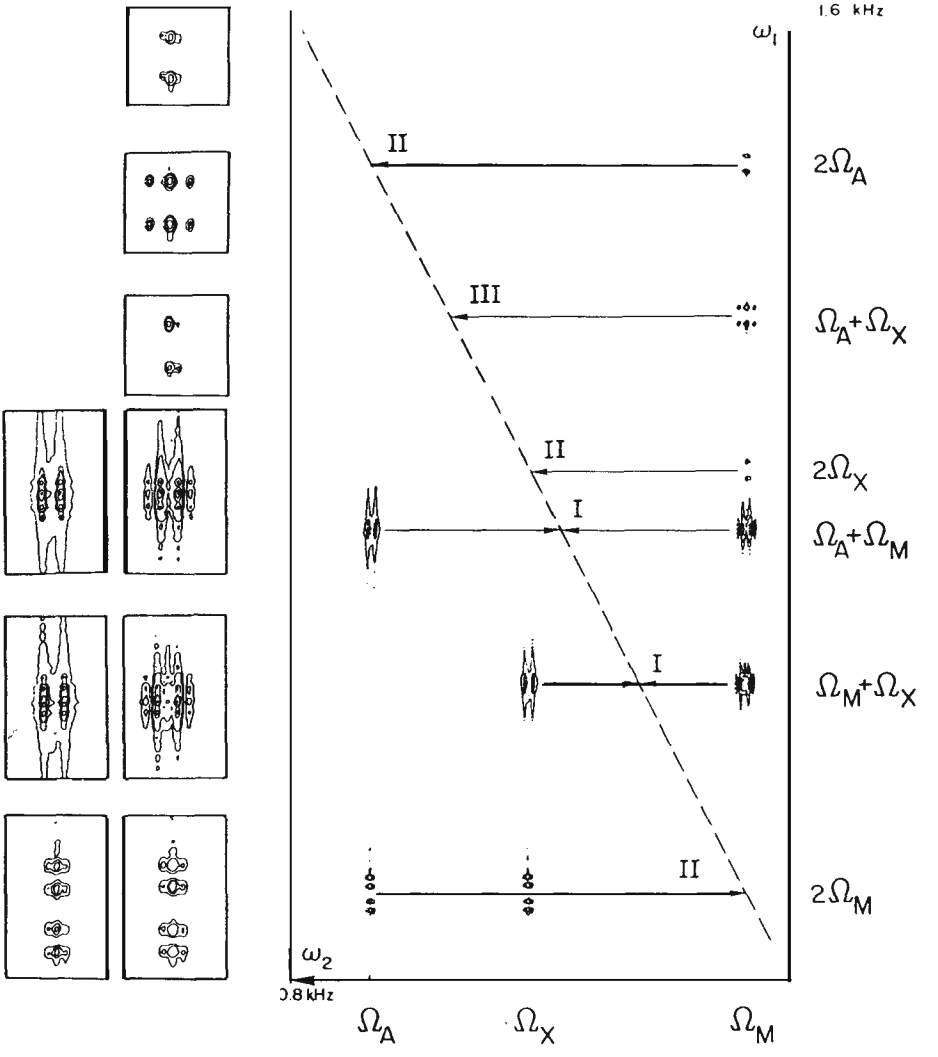

Figure 16. 90 MHz 2D correlation spectrum of 3-amino-propanol-d_3 with double quantum transitions along ω_1 and single quantum transitions along ω_2. The three categories I, II, and III of double quantum transitions mentioned in the text are indicated. Blow-ups of all cross peaks are shown on the left. The spectrum is shown in an absolute value representation (from Ref.89).

beautiful and useful form of a double quantum experiment is 2D INADEQUATE spectroscopy proposed by Bax, Freeman and Kempsell (90,91). There, only type I peaks can occur.

The methods mentioned so far produce additional cross peaks that provide information not accessible with the standard COSY and NOESY experiments. In the following, techniques are discussed that lead to simplified spectra which may facilitate their interpretation.

Multiple Quantum Filtering

A selective filtering effect can be achieved by exciting intermediately multiple quantum coherence, selecting a particular quantum order, and reconverting the selected order into observable magnetization. Depending on the selected order, this leads to multiple-quantum filtering of various orders. The spin-system-selective effect relies on coherence transfer selection rules that limit the allowed transfers for weakly coupled spins (8,92):

(i) It is impossible to excite p-quantum coherence in spin systems with less than p coupled spins $I = 1/2$.

(ii) For the appearance of a diagonal peak of spin I_k in a p-quantum filtered COSY spectrum, the spin I_k must be directly coupled to at least p-1 further spins.

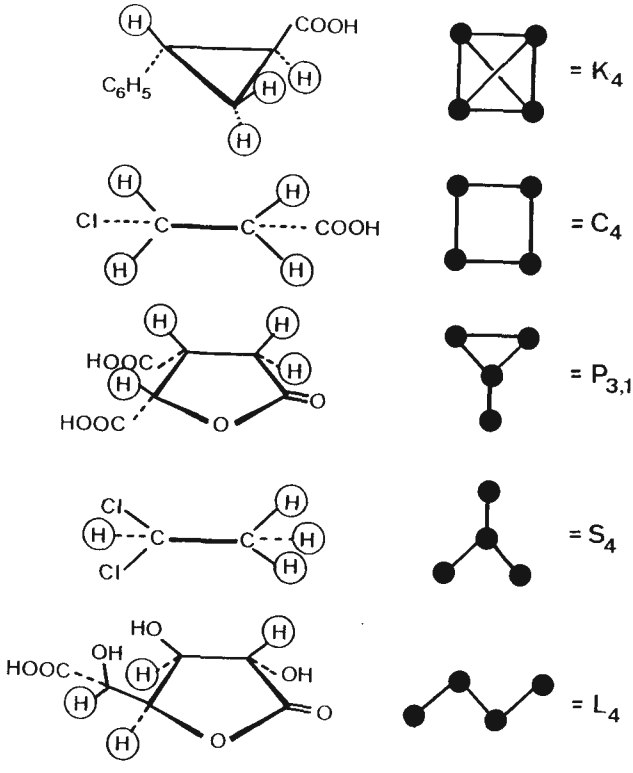

(iii) For the appearance of the cross peaks between spins I_k and I_l in a p-quantum filtered COSY spectrum, both spins must simultaneously be coupled to at least p-2 further spins.

Violations of these coherence transfer selection rules occur for strong coupling and for certain special relaxation situations (93).

In Fig. 17, the effect of 4-quantum filtering on various four-spin systems is demonstrated. The sample consists of the five molecules trans-phenylcyclopropanecarboxylic acid (K_4), DL-isocitric acid-lactone ($P_{3,1}$), 1,1-dichloroethane (S_4), 2-chloropropionic acid (C_4), and D-saccharic acid-l, 4-lactone (L_4) with the coupling topologies shown on the previous page (94).

Figure 17a gives a conventional (double-quantum-filtered) COSY spectrum of the mixture while in Fig. 17b the corresponding 4-quantum filtered spectrum is reproduced. The filtering effect can easily be understood based on the given rules and the shown coupling topologies. The interpretation is left to the reader. Only cross peaks of the molecule with K_4 topology and diagonal peaks of molecules with $P_{3,1}$, S_4, and K_4 topology remain.

Technically, multiple quantum filtering exploits the characteristic dependence of a multiple quantum coherence transfer on the rf phase of the acting pulse sequence (8,92,95,96). Let us assume a transfer of coherence $c_{p1}(t)$ by a unitary transformation U(O), representing a particular pulse sequence, to coherence $c_{p2}(t)$, where p_1 and p_2 are the orders of coherence,

$$c_{p1}(t) \xrightarrow{U(0)} c_{p2}(t). \qquad [14]$$

All rf pulses in the sequence shall now be phase-shifted by Φ, leading to $U(\Phi)$. Then it can be shown that the resulting coherence $c_{p2}(t)$ is phase-shifted by $(p_2 - p_1)\Phi$

$$c_{p1}(t) \xrightarrow{U(\Phi)} c_{p2}(t) \exp\{i(p_2 - p_1)\Phi\}. \qquad [15]$$

The phase shift is therefore proportional to the change in coherence order $\Delta p = p_2 - p_1$. After performing a series of experiments with the phase Φ incremented in regular intervals $2\pi/N$ from 0 to $2\pi(N-1)/N$, it is possible to select for a particular Δp by computing the corresponding Fourier coefficient of Δp: Let $s(t,\Phi)$ be the recorded signal of an experiment with phase shift Φ, then we obtain the filtered signal

$$s(t, \Delta p) = \sum_{k=0}^{N-1} s(t, 2\pi k/N) \exp(-i2\pi k \Delta p/N). \qquad [16]$$

The required number of increments N of the phase Φ depends on the number of Ap values that have to be discriminated (96). It is obvious that unless the initial order of coherence p_1 is known, no particular order of coherence p_2 can be filtered out in this manner. Most conveniently the initial state is selected to be in thermal equilibrium with $p_1 = 0$. Then, the entire pulse sequence preceding the point at which a coherence order

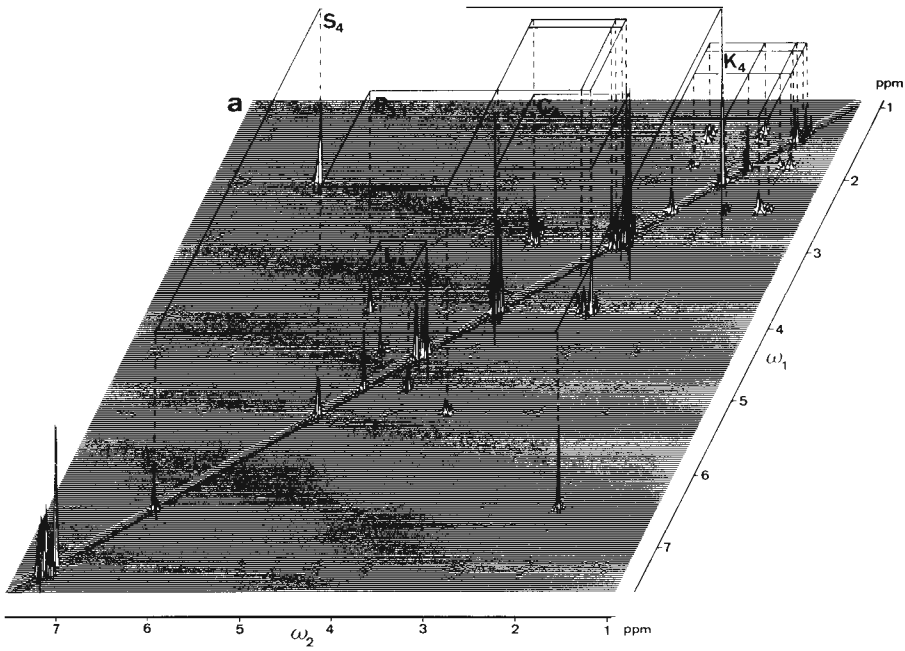

Figure 17. Multiple quantum-filtered and spin-topology-filtered 300 MHz COSY spectra of a mixture of the four-spin systems trans-phenyl cyclopropanccarboxylir acid (K_4), DL.-isocitric acid-lactone ($P_{3,1}$), 1,1-dichloroethane (S_4), 2-chloro-propionic acid (C_4), and D-saccharic acid-1,4-lactone (L_4). (a) Double-quantum-filtered spectrum using the pulse sequence of Fig. 18. (b) 4-quantum-filtered spectrum using the pulse sequence of Fig. 18. (c) C_4 spin-topology-filtered spectrum using the pulse sequence of Fig. 19 (from Ref. 94).

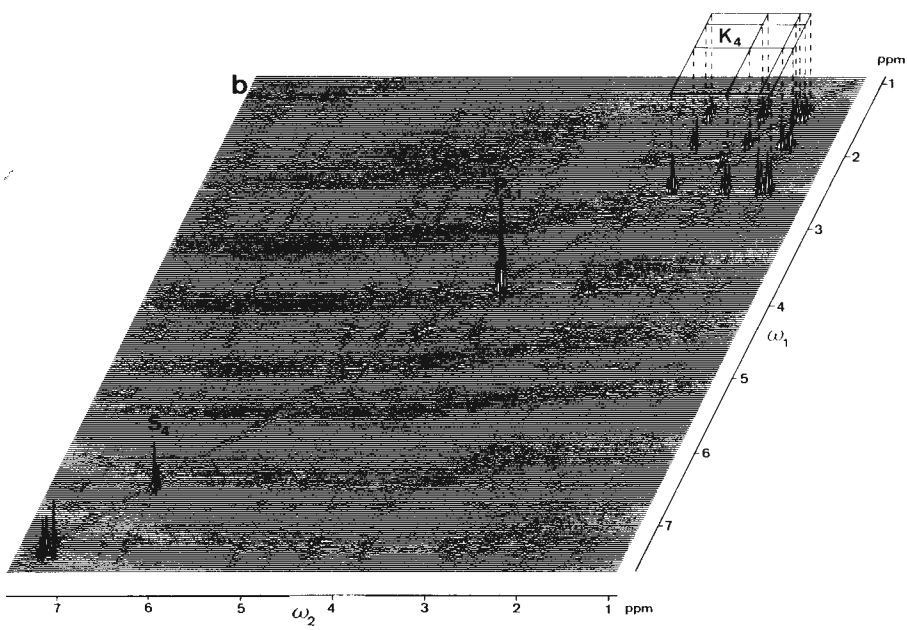

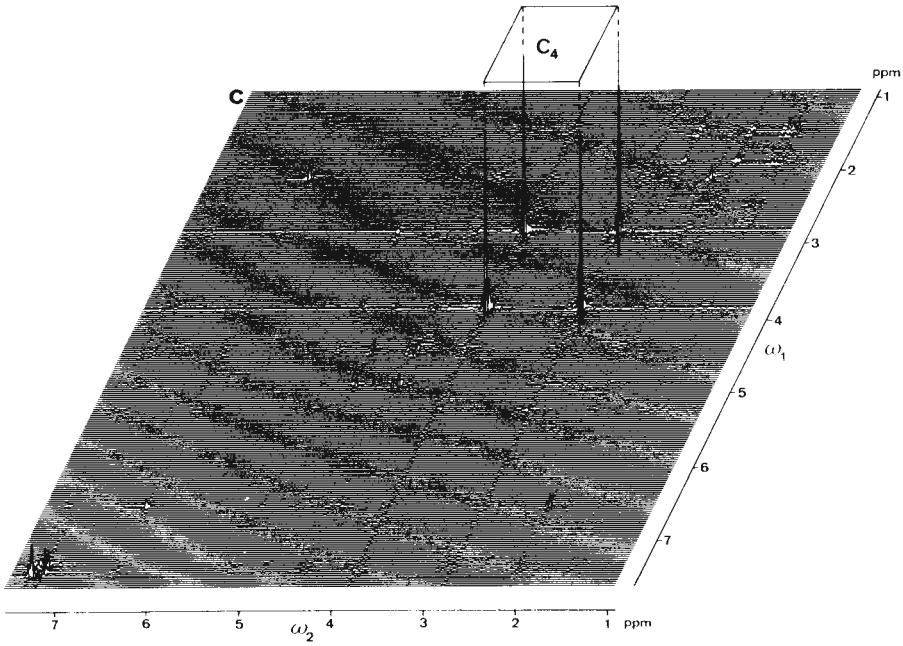

should be selected must be phase-cycled. For multiple-quantum filtered COSY, this leads to the pulse sequence shown in Fig. 18.

Obviously, multiple quantum filtering and phase-cycling require N-times more experiments to be performed. However, no information is lost as in each term of Eq. [16] just the phase factor is compensated and identical signals are co-added for the relevant pathways. Thus the longer performance time is refunded in terms of an increased signal-to-noise ratio.

Spin Topology Filtration

It may be desirable to enhance the filtering effect demonstrated in Fig. 17 and to select individual spin coupling topologies. Indeed it is possible to design extended pulse sequences, in combination with multiple quantum filtration, that are tailor-made for specific spin coupling topologies (94, 97, -98). A pulse sequence, built into a 2D COSY experiment, that is selective for cyclic C_4 spin coupling topologies is shown in Fig. 19. Applied to the previous mixture of four-spin systems, the 2D spectrum of Fig. 17c is obtained. It shows efficient suppression of all other spin systems. It should however be noted that the situation is here rather ideal. Often, these filters do not perform as well because their design relies on the equality of all non-zero spin couplings. In reality, there are weak and strong couplings that cannot be characterized by topological considerations alone. Often also the signals decay during the extended pulse sequences due to relaxation. This limits the practical usefulness of these designs.

Exclusive Correlation Spectroscopy

Multiple quantum filtering suppresses not only diagonal and cross peaks in 2D spectra but also changes the sign pattern in the cross-peak multiplet

structure. By appropriate combination of differently multiple-quantum filtered 2D spectra, it is possible to simplify the multiplet structure by reducing the number of multiplet components. The recipe of exclusive correlation spectroscopy (E.COSY), proposed by O.W. Sørensen, eliminates all multiplet components from a COSY spectrum except for those belonging to pairs of transitions with an energy level in common (99-101). In practice, it is not necessary to literally combine multiple-quantum-filtered spectra but it is possible to directly co-add the experimental results from a phase cycle with the appropriate weight factors.

Figure 20 shows schematically the combination of cross-peak multiplets connecting spins I_1 and I_2 in a three-spin system after 2- and 3-quantum filtering. The remaining pattern consists of two basic squares with side lengths equal to the active coupling constant J_{12} responsible for the coherence transfer. The displacement vector between the two squares is given by the two passive couplings J_{13} and J_{23} to the third (passive) spin. It should be mentioned that this multiplet structure is identical to the one obtained by a COSY experiment with an extremely small flip angle of the mixing pulse (102).

E.COSY is of practical use whenever the cross-peak multiplet structure has to be analyzed in order to determine J-coupling constants. This can be done conveniently by hand by measuring the displacement of peripheral multiplet components (101) or by an automatic recursive contraction procedure (103).

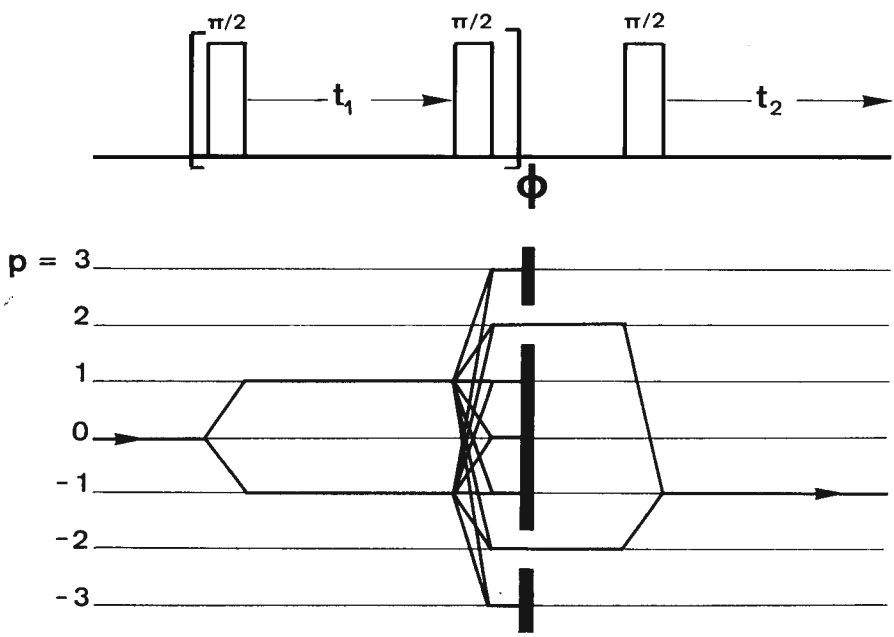

Figure 18. Pulse sequence for multiple-quantum-filtered COSY with the coherence transfer diagram for double-quantum filtering. The phase Φ is incremented systematically in a set of N experiments and the resulting experimental results combined according to Eq. [16].

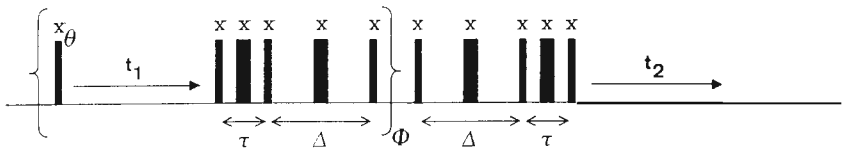

Figure 19. Pulse sequence for C_4 spin topology filtration consisting of π/2 and π pulses. The delays are adjusted to $\tau = 1/(8J)$ and $\Delta = 1/(2J)$ where J is the uniform J-coupling constant. Φ is phase-cycled for four-quantum selection and Θ for the suppression of axial peaks (94).

Heteronuclear 2D Experiments

In addition to the homonuclear 2D experiments discussed so far, at least an equal number of heteronuclear experiments has been proposed and introduced in the routine spectroscopy laboratory. Of greatest practical importance are heteronuclear shift correlation spectra that correlate the chemical shifts of directly bonded or remotely connected heteronuclei (104, 105). In this context, so-called inverse detection experiments where proton I-spin coherence is observed in t_2 while low-abundance, low sensitivity S-spin coherence is evolving in t_1, are of particular interest (104). The most efficient schemes create heteronuclear two-spin coherence that evolves in t_1 and that acquires the frequency information of the S-spin resonance (106). Also in the heteronuclear environment, relayed coherence transfer is of importance (78) as well as experiments in the rotating frame (107). Spin filtering is used in the form of multiplicity selectivity, distinguishing S spins coupled to one, two, or three I spins (1 OS), and in the form of J filtering for the distinction of one-bond and multiple-bond couplings (109). This enumeration of heteronuclear experiments is by no means exhaustive.

THREE-DIMENSIONAL FOURIER SPECTROSCOPY

No new principles are required to develop 3D spectroscopy that is just a logical extension of 2D spectroscopy. Instead of a single mixing process which relates two frequency variables, two sequential mixing processes relate three frequencies: the origin frequency ω_1 the relay frequency ω_2, and the detection frequency ω_3, as shown in Fig.21. In this sense, a 3D experiment can be considered as the combination of two 2D experiments. Obviously, a very large number of possible 3D experiments can be conceived. However, only few of them have so far proved to be indispensible (110-118).

Two applications of the 3D spectroscopy concept have emerged: (i) 3D correlation and (ii) 3D dispersion (see also Fig.13). Three-dimensional correlation is of importance in homonuclear experiments. It has been mentioned that the assignment procedure in biomolecules requires a COSY-type and a NOESY-type 2D spectrum. The two 2D experiments could be contracted into one 3D experiment, combining a J-coupling-mediated and a cross-relaxation transfer. A 3D COSY-NOESY spectrum possesses the advantage that the entire assignment process can be carried

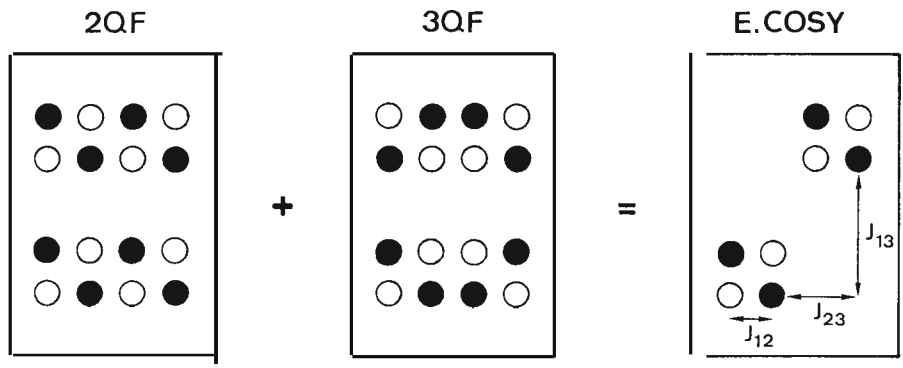

Figure 20. E.COSY experiment to simplify the multiplet structure of cross peaks. The double-quantum- and the triple-quantum-filtered cross peak between spins I_1 and I_2 of a three-spin system are combined to produce an E.COSY pattern. Positive and negative multiplet components are distinguished by empty and filled circles.

out with a single homogeneous data set (115, 116). It incorporates also redundancies that allow cross checks of the assignments. For obtaining quantitative information, however, 3D spectra are less suited as all peak intensities are products of two transfer coefficients that are some times difficult to separate.

A 3D ROESY-TOCSY spectrum of the linear nonapeptide buserilin is shown in Fig.22 (116). A ROESY instead of a NOESY step is required for buserilin, being a molecule of intermediate size where the NOE intensities are small. The TOCSY step has the advantage that chains of multiple-step cross peaks extending into the side chains are obtained that facilitate the identification of the amino acid residues.

It should be recognized that recording a 3D spectrum is considerably more time-consuming than two 2D spectra as two time parameters t_1 and t_2 have to be incremented independently, leading to a 2D array of experiments. Here the question arises; when is it worth the effort to record a 3D spectrum? This question has been discussed before (116, 119, 120).

Let us consider a particular cross peak in a 3D spectrum that correlates the coherences {tu} in ω_1, {rs} in ω_2, and {pq} in ω_3 dimensions. Its intensity is determined by the following product of matrix elements (in the eigenbasis of the unperturbed Hamiltonian $\mathcal{H}_0$) (116):

$$Z_{\{pq\}\{rs\}\{tu\}} = D_{qp}\, R^{(2)}_{\{pq\}\{rs\}}\, R^{(1)}_{\{rs\}\{tu\}}\, (\hat{\hat{P}}\sigma_0)_{tu}. \qquad [17]$$

A non-vanishing intensity establishes a two-step correlation {tu}-{rs}-{pq}.

The 3D experiment can be compared with two 2D experiments that employ the mixing processes $\hat{\hat{R}}^{(1)}$ and $\hat{\hat{R}}^{(2)}$, respectively. The corresponding intensities would be

$$Z^{(1)}_{\{rs\}\{tu\}} = D^{(1)}_{sr} R^{(1)}_{\{rs\}\{tu\}}\, (\hat{\hat{P}}\sigma_0)_{tu}. \qquad [18]$$

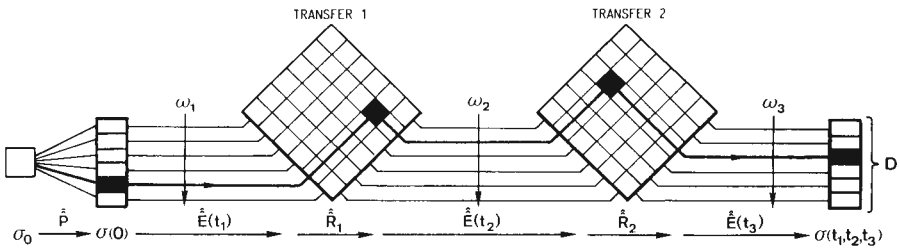

Figure 21. Schematic representation of a 3D experiment, extending Figs. 1 and 6. Three evolution periods with the time variables t_1 t_2, and t_3 are separated by two transfer or mixing processes. A 3D experiment can be conceived as the contraction of two 2D experiments.

$$\text{and } Z^{(2)}_{\{pq\}\{rs\}} = D_{qp}\, R^{(2)}_{\{pq\}\{rs\}}\, (\hat{\mathbf{P}}^{(2)}\sigma_0)_{rs}. \qquad [19]$$

When in the 2D spectra the two relevant peaks with intensities $Z^{(1)}_{\{rs\}\{tu\}}$ and $Z^{(2)}_{\{pq\}\{rs\}}$ can be identified, possibly in crowded regions, the two-step correlation, represented by a 3D peak, could also be established based on the two 2D spectra {tu}-{rs} and {rs}-{pq}. Provided that $Z_{\{pq\}\{rs\}\{tu\}} \neq 0$, the intensities $Z^{(1)}_{\{rs\}\{tu\}}$ and $Z^{(2)}_{\{pq\}\{rs\}}$ are different from zero when in addition $D^{(1)}_{sr} \neq 0$ and $(\hat{\mathbf{P}}^{(2)}\sigma_0)_{rs} \neq 0$. This implies that the "relay-transition" {rs} must be excited in the preparation state $P^{(2)}$ and must be detectable by the observable $D^{(1)}$. For "allowed" one-spin single-quantum coherences, this condition is fulfilled for single pulse excitation and direct detection. On the other hand, "forbidden" multiple-spin single-quantum coherences (combination lines) and multiple-quantum coherences can neither be excited by a single non-selective pulse nor directly detected. Such coherences regularly occur in the ω_2-dimension of a 3D spectrum. The excitation and indirect detection of these coherences in 2D experiments requires special excitation and detection pulse sequences.

In conclusion, the two constituent 2D experiments deliver the same information on the spin system as the 3D spectrum, provided that (i) the relevant frequencies in the ω_2-dimension of the 3D spectrum can be excited and detected in the 2D experiments, and (ii) the cross-peaks are not hidden by spectral overlap and can be identified in the 2D spectra. The first condition is normally not severe as the 2D experiments can be modified for excitation and detection of forbidden transitions whenever required. On the other hand, the limited resolving power of 2D spectra is the most important motivation for justifying 3D (and possibly higher dimensional) spectroscopy.

Because the gain in resolution justifies 3D spectroscopy, it may be worthwhile to introduce a third frequency axis just for resolution purposes, rather than combining two processes relevant for the assignment requiring high resolution in all three dimensions. It is then possible to arbitrarily choose the extent of 3D resolution and to optimize the performance time of the 3D experiment. For the 3D spreading of a 2D spectrum, homonuclear or heteronuclear transfers can be used. Heteronuclear one-bond transfers

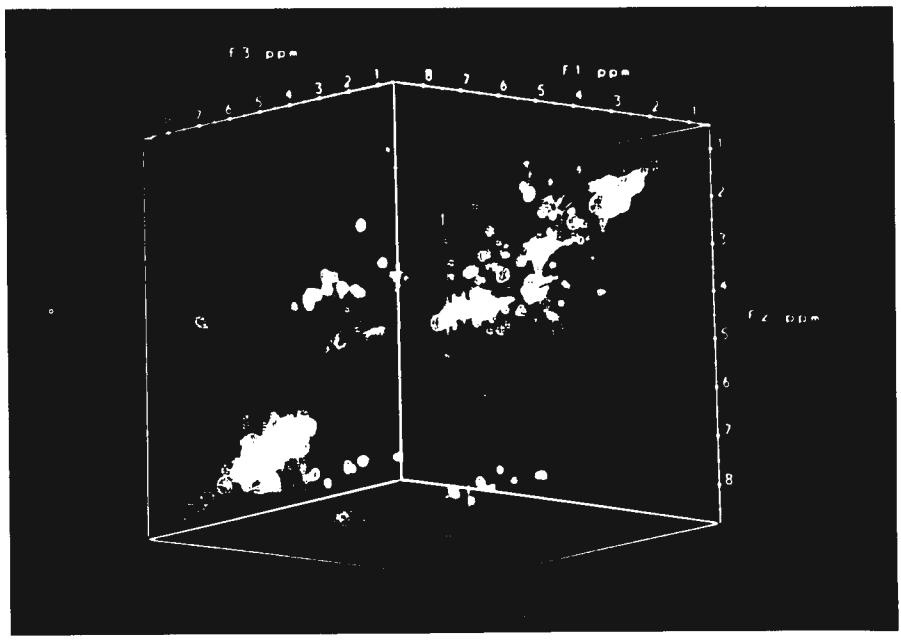

Figure 22. 3D **view of a 300 MHz *3D* homonuclear ROESY-TOCSY spectrum of buserilin in DMSO-d_6 photographed from a picture system (116).**

are however far more efficient because the strong heteronuclear one-bond couplings prevent leakage to further spins. This allows an efficient transfer, virtually without loss of magnetization. In addition, nuclei like ^{13}C and ^{15}N exhibit large chemical shift ranges with high resolving power. The principle of spreading is indicated in Fig. 23.

A 3D ^{15}N-spreaded TOCSY spectrum of ribonuclease A is shown in Fig.24. The use of heteronuclear spreading requires usually isotopic labelling of the molecule. In this case, ribonuclease A has been grown in a ^{15}N-labelled nutrients-containing E.Coli medium (courtesy of Prof. Steven Benner). The spectrum has been obtained with the pulse sequence of Fig.25. Initially, proton coherence is excited and precesses during t_1 under ^{15}N refocusing by the applied π pulse. During the mixing time τ_m, coherence transfer from other protons to the NH protons is effected in the rotating frame by the application of a TOCSY multiple-pulse sequence. The NH coherence is then converted into ^{15}NH heteronuclear multiple-quantum coherence (HMQC) which precesses during t_2 and acquires ^{15}N resonance information (under proton refocusing). After reconversion into NH proton coherence, detection follows during t_3 under ^{15}N decoupling. For a complete assignment of the proton resonances, in addition a ^{15}N-spreaded NOESY spectrum is required.

The step to 4D spectroscopy (121) is a small and logical one: in 2D experiments, spins are pairwise correlated, e.g. NH and $C_\alpha H$ protons. Three-dimensional dispersion uses either ^{15}N or $^{13}C_\alpha$ resonance for spread-

ing the resonances of NH or $C_\alpha H$, respectively. In a 4D experiment, both spreading processes are applied simultaneously:

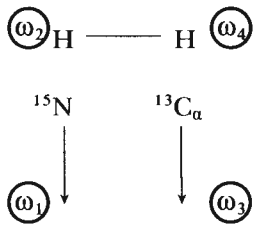

The order of the frequencies in the actual experiment is a matter of convenience. Normally, the detection frequency ω_4 refers to proton spins for sensitivity reasons. In most cases, the two spreading coordinates are rather coarsely digitized to limit the performance time, just enough to achieve separation of peaks overlapping in the 2D spectrum. Often 8 to 32 points in each of the two dimensions are sufficient.

MOLECULAR DYNAMICS INVESTIGATED BY NMR

The molecular structures, determined by NMR in solution, by X-ray diffraction in single crystals, or by other means, are invariably motionally averaged structures, whereby the averaging process is strongly dependent on the measurement technique. To interpret experimental "structures", some knowledge of the motional properties of the molecule is in fact indispensible. Molecular dynamics is also relevant for its own sake, in particular for understanding reactivity and interaction with other molecules. In many cases, active sites in a molecular pocket are only accessible due to the flexibility of the molecule itself.

The characterization of the motional properties of a molecule is by orders of magnitude more difficult than the description of an averaged molecular structure. While 3N-6 coordinates are sufficient to fix a structure containing N atoms, the characterization of molecular dynamics requires 3N-6 variances of the intramolecular coordinates, (3N-6)(3N-5)/2 covariances, and the same number of auto- and cross-correlation functions, respectively. In addition, also higher order correlation functions are needed for a more refined description of dynamics. In practice, a sufficient number of observables is never available for a full description of dynamics. In this sense, the study of dynamics is an open-ended problem. Numerous techniques are available to obtain data on dynamics: Debye-Waller factors in X-ray diffraction give hints on the variances of the nuclear coordinates, however without a measure for the time scale. Inelastic and quasi-elastic neutron scattering deliver correlation functions, but without a reference to the structure. Fluorescence depolarization allows one to determine the motional correlation function of fluorescent groups, such as tyrosine residues in proteins. Ultrasonic absorption gives an indication of the dominant motional mode frequencies, again without a structural reference.

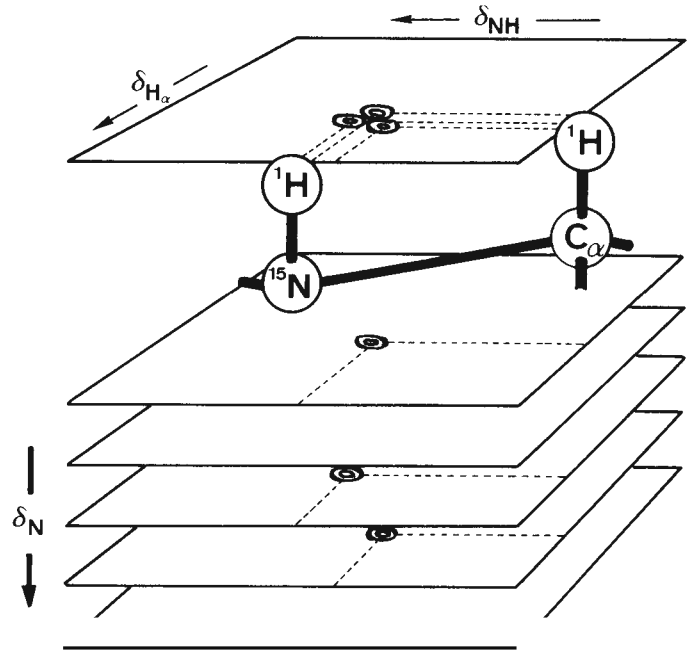

Figure 23. 3D resolution of a 2D proton-resonance spectrum by ^{15}N resonance spreading. The NH-C_αH cross peaks are displaced in a third dimension by the corresponding ^{15}N chemical shifts.

NMR is more universally applicable to motional studies than most of the other techniques. The range of correlation times τ_c that can be covered by various NMR methods is enormous, from picoseconds to seconds and more:

$1\ s < \tau_c$:	Real time monitoring after initial perturbation
$10\ ms < \tau_c < 10\ s$:	2D exchange spectroscopy (EXSY)
$100\ \mu s < \tau_c < 1\ s$:	Line shape effects, exchange broadening and exchange narrowing
$1\ \mu s < \tau_c < 10\ ms$:	Rotating frame $T_{1\rho}$ relaxation measurements
$30\ ps < \tau_c < 1\ \mu s$:	Laboratory frame T_1 relaxation
$\tau_c < 100\ ps$:	Averaged parameter values .

Except for slow motions on a millisecond or slower time scale where lineshape, saturation transfer, and 2D exchange studies can be performed, many dynamics studies by NMR rely on relaxation measurements. The various relaxation parameters, such as the longitudinal relaxation time T_1, the transverse relaxation time T_2, the rotating frame relaxation time $T_{1\rho}$, and cross-relaxation rate constants Γ_{kl}, depend on the correlation time τ_c of the underlying random process.

The discussion shall be restricted to a recent study of the intramolecular dynamics in antamanide (I) (83, 122, 123) (see Figs. 8, 9, 11). Antamanide is an antidote for toxic components of the mushroom *Amanita phalloides.*

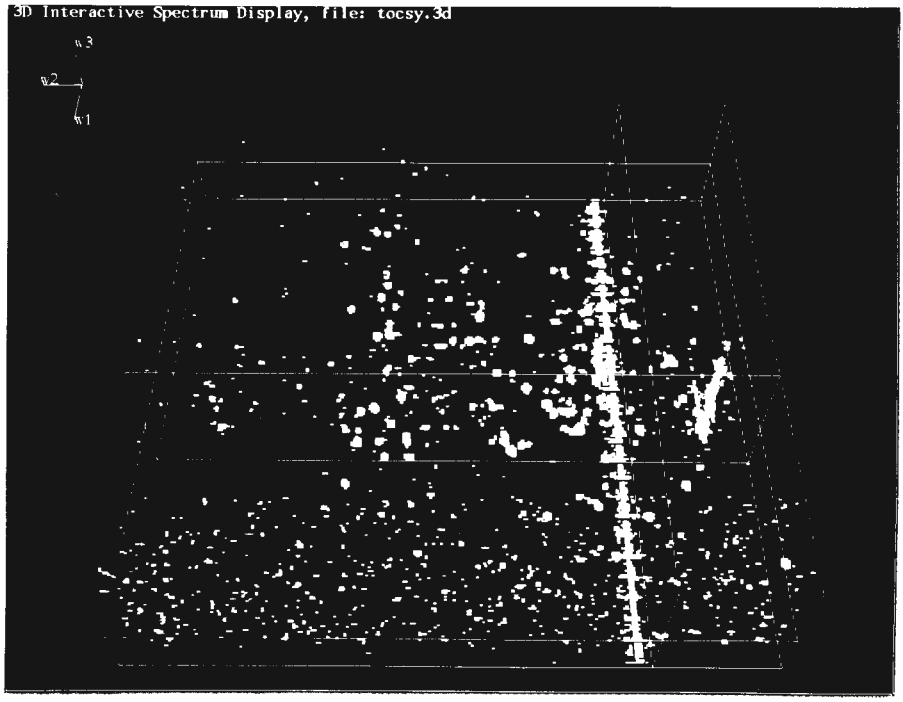

Figure 24. 3D ^{15}N-spreaded 600 MHz proton resonance TOCSY spectrum of ^{15}N-labelled ribonuclease A in H_2O solution. The 3D spectrum shows the ^{15}N resonances along the ω_2 axis. The spectrum has been recorded by C. Griesinger, using the pulse sequence of Fig. 25, and processed by S. Boentges. The sample was provided by Prof. S. Benner of ETH Zürich.

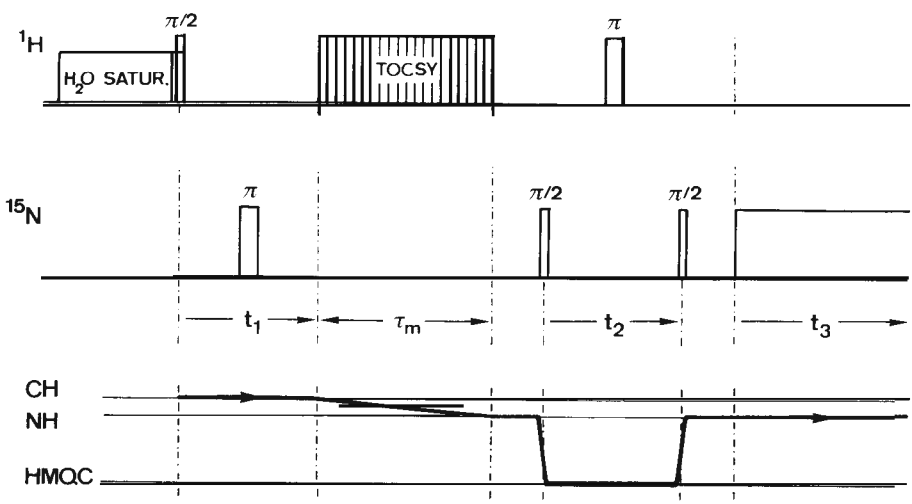

Figure 25. Pulse sequence for recording a 3D ^{15}N-spreaded TOCSY spectrum. After presaturation of the water resonance, proton resonance is excited and precesses during t_1. After the homonuclear TOCSY transfer from CH to NH protons, the coherence is converted into heteronuclear multiple quantum coherence (HMQC) that evolves during t_2 and acquires ^{15}N shift information. After reconversion to proton coherence, NH resonance is detected during t_3 under ^{15}N decoupling.

Astonishingly, the antidote occurs as a component of the same mushroom. Indications have been found in early ultrasonic absorption studies (124) that the peptide ring seems to undergo a conformational exchange process with a frequency of about 1 MHz. In the course of extensive investigations of antamanide by the research group of Professor Horst Kessler (125), it has also been noticed that the distance constraints obtained from NMR measurements could not be fitted by a single conformation. Martin Blackledge has performed in our laboratory rotating frame relaxation measurements and localized a hydrogen-bond exchange process with an activation energy of 25 kJ/mol and a lifetime of 25 μs at room temperature (unpublished results, see also Ref. 126). With a new dynamic structure determination procedure, called MEDUSA (123), the conformational space of antamanide has been investigated more systematically than ever before. 1176 feasible low-energy structures have been found. They have been combined in dynamically interchanging pairs in an attempt to fulfill all experimental constraints that consist of NOE distance constraints, J-coupling angular constraints and specific information on hydrogen bond dynamics. A large set of feasible structural pairs has been constructed. Many pairs are within experimental accuracy compatible with the experimental data. For a more restrictive description of the dynamic system of antamanide, additional and more accurate experimental data are required. Figure 26 shows, as an example, the dynamic pair of structures that so far fits the experimental data best. The two interconverting structures differ primarily in the hydrogen bonds $Val^{1}NH$-$Phe^{9}O$ and $Phe^{6}NH$-$Ala^{4}O$, that exist only in one of the two conformations, and in the torsional angles φ_5 and φ_{10}.

A second study concentrated on the ring puckering dynamics of the four proline residues in antamanide (122). The conformation of the five-ring systems can be determined from the dihedral bond angles χ_1, χ_2, and χ_3 that in turn can be deduced from the vicinal proton-proton J-coupling constants using the Karplus relations (54). The relevant coupling constants (21 per residue) have been determined from E.COSY spectra. Based on these measurements, a model was constructed for each of the proline residues by least squares fitting. It was found that for Pro^{3} and Pro^{8} a good fit can be obtained with a single rigid conformation, while for Pro^{2} and Pro^{7} two rapidly exchanging conformations were required to reduce the fitting error into an acceptable range. At the same time, ^{13}C relaxation-time measurements confirmed that Pro^{3} and Pro^{8} appear to be rigid while Pro^{2} and Pro^{7} show dynamics with correlation times between 30 and 40 ps. This implies that the peptide ring dynamics and the proline ring dynamics are not correlated and proceed on entirely different time scales. The two exchanging conformations that have been found for Pro^{2} are shown in Fig. 27. It is seen that the motion involves an envelope-type process where the 'flap of the envelope' (Cγ) is moving up and down.

MAGNETIC RESONANCE FOURIER IMAGING

Magnetic resonance imaging (MRI) has had an enormous impact on medical diagnosis and became rapidly a powerful routine tool. The basic procedure for recording a 2D or 3D NMR image of an object is due to Paul Lauterbur (127). A magnetic field gradient, applied along different directions in space in a sequence of experiments, produces projections of the nuclear spin density of the object onto the direction of the gradient. From a sufficiently large set of such projections it is possible to reconstruct an image of the object, for example by filtered backprojection in analogy to X-ray tomography.

A different approach is directly related to 2D and 3D Fourier transform spectroscopy. Frequency encoding of the three spatial dimensions is achieved by a linear magnetic field gradient applied successively along three orthogonal directions for the durations t_1, t_2, and t_3, respectively, in a pulse Fourier transform experiment (128). In full analogy to 3D spectroscopy, the time parameters t_1 and t_2 are incremented in regular intervals from experiment to experiment. The recorded signal $s(t_1,t_2,t_3)$ is Fourier-transformed in three dimensions to produce a function $S(\omega_1,\omega_2,\omega_3)$ that is equivalent to a 3D spatial image when the spatial information is decoded using the relations $x = \omega_1/g_x$, $y = \omega_2/g_y$, and $z = \omega_3/g_z$ with the three field gradients g_x, g_y, and g_z. The procedure is illustrated in Fig. 28 for two dimensions.

In a further refinement, proposed by Edelstein et al. (129), the time variables t_1 and t_2 are replaced by variable field gradient strengths g_x and g_y applied during a constant evolution time. With regard to the accumulated phase,

$$\gamma = x\, g_x t_1 + y\, g_y t_2 + z\, g_z t_3, \qquad [20]$$

it is immaterial whether the evolution time or the field gradients are varied. However, keeping the time t_k constant eliminates undesired relaxation effects.

In medical imaging, 3D experiments have a natural justification, although it is sometimes simpler to apply selective excitation techniques to select a 2D slice through the object to be imaged (130). Even extensions to higher dimensions are quite realistic. In a fourth dimension, for example, chemical shift information can be accommodated (131). Also 2D spectroscopic information could be combined with three spatial dimensions, leading to a 5D experiment. No limitations seem to exist for the human imagination. However, the practical limits will soon be reached when the required performance times is also taken into consideration.

CONCLUSION

I am not aware of any other field of science outside of magnetic resonance that offers so much freedom and opportunities for a creative mind to invent and explore new experimental schemes that can be fruitfully applied in a

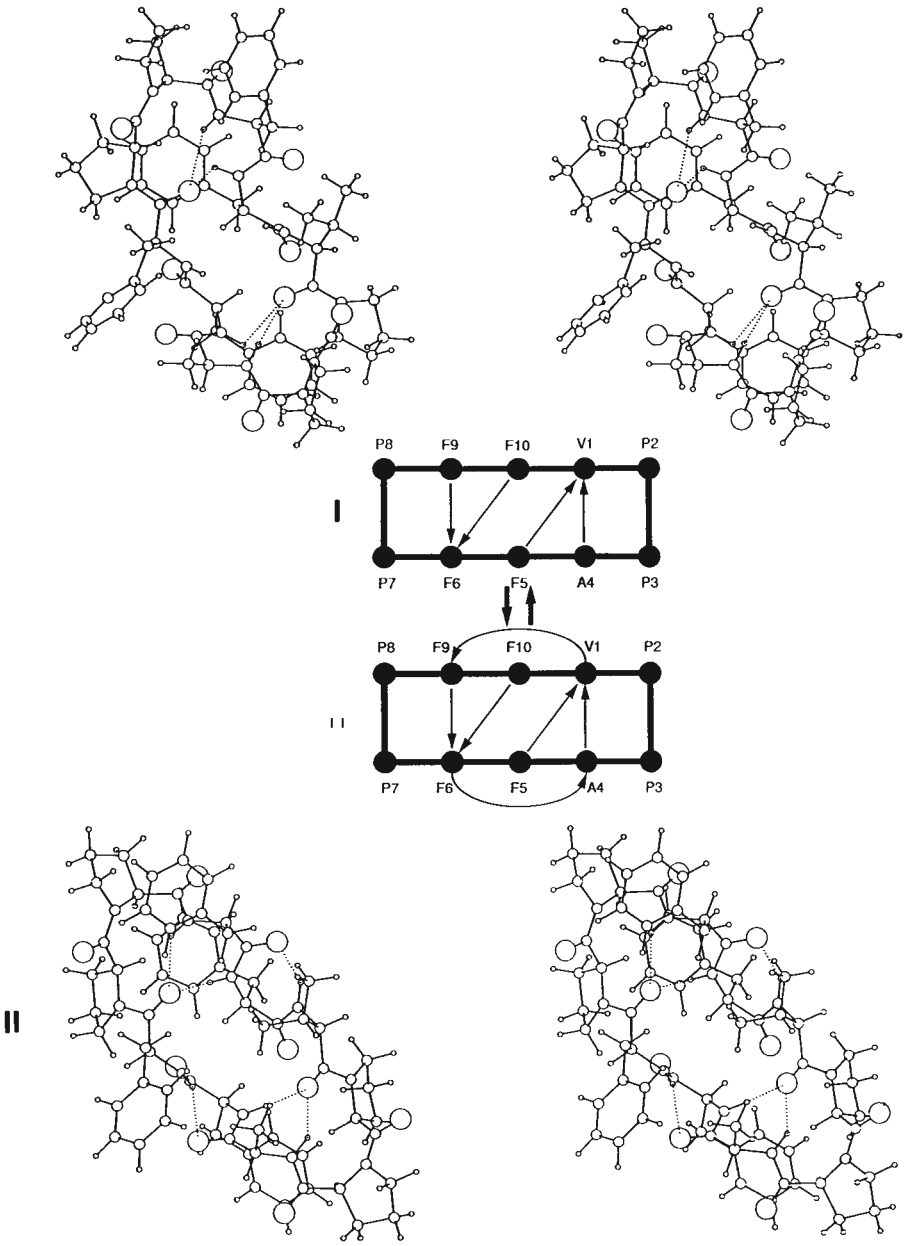

Figure 26. **Conformational pair of antamanide that fulfills the experimental constraints. The two pairs are shown in stereographic as well as in abstract form. In the former, hydrogen bonds are indicated by broken lines, in the latter by arrows pointing towards the hydrogen-bonded oxygen (from Ref. 123).**

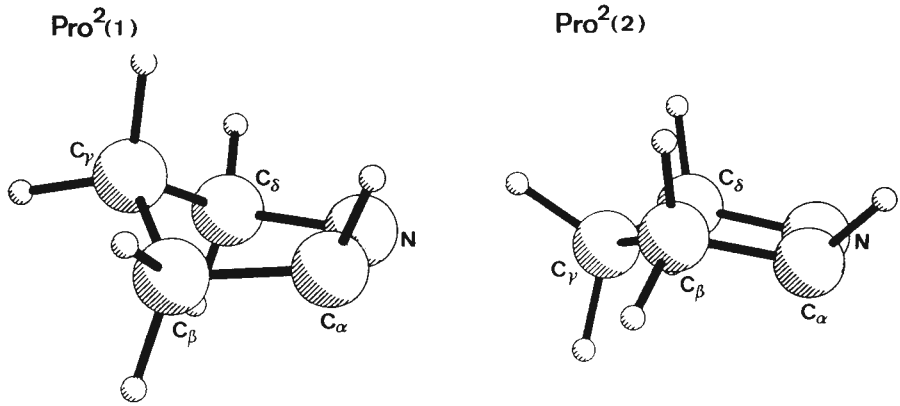

Figure 27. The two experimentally determined conformations of probe-2 in antamanide (see Ref. 122).

variety of disciplines. NMR is intellectually attractive because the observed phenomena can be understood based on a sound theory, and almost all conceits can also be tested by easy experiments. At the same time, the practical importance of NMR is enormous and can justify many of the playful activities of an addicted spectroscopist.

ACKNOWLEDGMENTS

Most of the credit for the inspiration and execution of the work described should go to my teachers Hans Primas and Hans H. Günthard, to my supervisor Weston A. Anderson, to the inspirator Jean Jeener, to my coworkers (in more or less chronological order): Thomas Baumann, Enrico Bartholdi, Robert Morgan, Stefan Schäublin, Anil Kumar, Dieter Welti, Luciano Müller, Alexander Wokaun, Walter P. Aue, Jiri Karhan, Peter Bachmann, Geoffrey Bodenhausen, Peter Brunner, Alfred Höhener, Andrew A. Maudsley, Kuniaki Nagayama, Max Linder, Michael Reinhold, Ronald Haberkorn, Thierry Schaffhauser, Douglas Burum, Federico Graf, Yongren Huang, Slobodan Macura, Beat H. Meier, Dieter Suter, Pablo Caravatti, Ole W. Sørensen, Lukas Braunschweiler, Malcolm H. Levitt, Rolf Meyer, Mark Rance, Arthur Schweiger, Michael H. Frey, Beat U. Meier, Marcel Müri, Christopher Councell, Herbert Kogler, Roland Kreis, Norbert Müller, Annalisa Pastore, Christian Schönenberger, Walter Studer, Christian Radloff, Albert Thomas, Rafael Bruschweiler, Herman Cho, Claudius Gemperle, Christian Griesinger, Zoltan L. Mádi, Peter Meier, Serge Boentges, Marc McCoy, Armin Stöckli, Gabriele Aebli, Martin Blackledge, Jacques Briand, Matthias Ernst, Tilo Levante, Pierre Robyr, Thomas Schulte-Herbrüggen, Jürgen Schmidt and Scott Smith; to my technical staff, Hansruedi Hager, Alexandra Frei, Janos A. Deli, Jean-Pierre Michot, Robert Ritz, Thomas Schneider, Markus Hintermann, Gerhard Gucher, Josef Eisenegger, Walter Lämmler, and Martin Neukomm; to my secretary Irene Müller; and to several research groups with which I had the pleasure to collaborate, first of all the research group of Kurt Wüthrich, and the

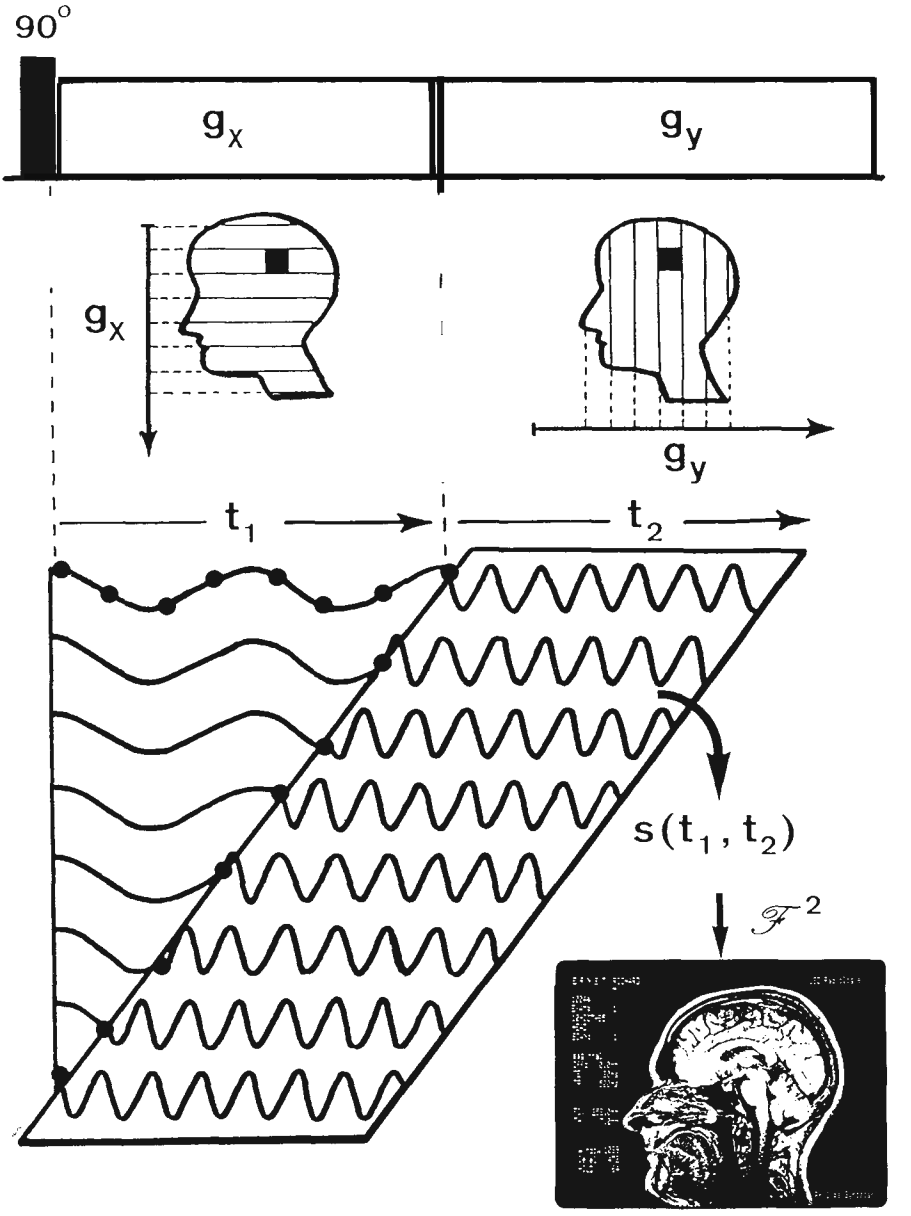

Figure 28. Schematic representation of Fourier NMR imaging, here shown in two dimensions. Two orthogonal gradients are applied during the t_1 and t_2 periods of a 2D experiment. A 2D Fourier transformation of the data set $s(t_1, t_2)$ produces a 2D image of the investigated subject (R.R.E.).

group of Horst Kessler. I also owe much gratitude for support in the early days to Varian Associates and more recently to the Swiss Federal Institute of Technology, the Swiss National Science Foundation, the Kommission zur Förderung der Wissenschaftlichen Forschung, and last but not least to Spectrospin AG.

REFERENCES

1. I.I. Rabi, Phys. Rev. 51, 652 (1937).
2. I.I. Rabi, J.R. Zacharias, S. Millman, and P. Kusch, Phys. Rev. 53, 318 (1938); I.I. Rabi, S. Millman, P. Kusch, J.R. Zacharias, Phys. Rev. 55, 526 (1939).
3. J.M.B. Kellogg, I.I. Rabi, N.F. Ramsey, and J.R. Zacharias, Phys. Rev. 55, 318 (1939); 56, 728 (1939); 57, 677 (1940).
4. E.M. Purcell, H.G. Torrey, and R.V. Pound, Phys. Rev. 69, 37 (1946).
5. F. Bloch, W. Hansen, and M.E. Packard, Phys. Rev. 69, 127 (1946).
6. F. Bloch, Phys. Rev. 70, 460 (1946).
7. J. Brossel and A. Kastler, C. R. Acad. Sci. 229, 1213 (1949); A. Kastler, J. Physique 11, 255 (1950).
8. R.R. Ernst, G. Bodenhausen, and A. Wokaun, *Principles of NMR in One and Two dimensions,* Clarendon Press, Oxford, 1987.
9. A. Bax, *Two-dimensional NMR in Liquids,* Delft University Press, D. Reidel Publ. Comp., Dortrecht, 1982.
10. Attur-ur Rahman, *Nuclear Magnetic Resonance, Basic Principles,* Springer, New York, 1986.
11. N. Chandrakumar and S. Subramanian, *Modern Techniques in High-resolution FT-NMR,* Springer, New York, 1987.
12. H. Friebolin, *Ein- und zwei-dimensionale NMR-Spektroskopie,* VCH-Verlag, Weinheim, 1988.
13. G.E. Martin and A.S. Zektzer, *Two-dimensional NMR Methods for Establishing Molecular Connectivity,* VCH Verlagsgesellschaft, Weinheim, 1988.
14. J. Schraml and J.M. Bellama, *Two-dimensional NMR Spectroscopy,* Wiley Interscience, New York, 1988.
15. W.S. Brey, ed., 'Pulse methods in 1D and 2D liquid-phase NMR', Academic Press, New York, 1988.
16. A.A. Michelson, Phil. Mag. Ser. 5, 31, 256 (1891); A.A. Michelson, *Light Waves and their Uses*, University of Chicago Press, Chicago, 1902.
17. P. Fellgett, Thesis, Cambridge University, 1951; P. Fellgett, J. Phys. Radium, 19, 187 (1958).
18. Varian Associates Magazine, 24, No.7, 11 (Aug. 1979); IEEE Center for the History of Electrical Engineering Newsletter No. 24, 2 (1990).
19. R.R. Ernst and W.A. Anderson, Rev. Sci. Instrum. 37, 93 (1966).
20. R.R. Ernst, Adv. Magn. Reson. 2, 1 (1966).
21. W.A. Anderson and R.R. Ernst, US Patent No. 3.475.680 'Impulse resonance spectrometer including a time averaging computer and a Fourier analyzer', filed May 26, 1965, issued Oct. 28, 1969.
22. R.R. Ernst, in *The Applications of Computer Techniques in Chemical Research,* The Institute of Petroleum, London, 1972, p.61.
23. O.W. Sørensen, G.W. Eich, M.H. Levitt, G. Bodenhausen, and R.R. Ernst, Prog. NMR Spectrosc. 16, 163 (1983).
24. J.B.J. Fourier, 'Theorie analytique de la chaleur', Firmin Didot, Pere et fils, Paris, 1822.
25. I.J. Lowe and R.E. Norberg, Phys. Rev. 107, 46 (1957).
26. N. Wiener, M.I.T. Radiation Lab., Rep.V-16S, Apr.6, 1942; N. Wiener, *Non-Linear Problems in Random Theory,* Wiley, New York, 1958.
27. R.H. Varian, US Patent No. 3.287.629 'Gyromagnetic resonance methods and apparatus', filed Aug. 29, 1956, issued Nov. 22, 1966.
28. H. Primas, Helv. Phys. Acta 34, 36 (1961).
29. R.R. Ernst and H. Primas, Helv. Phys. Acta 36, 583 (1963).
30. R.R. Ernst, J. Chem. Phys. 45, 3845 (1966).
31. R.R. Ernst, Mol. Phys. 16, 241 (1969).
32. R. Kaiser, J. Magn. Reson. 3, 28 (1970).

33. R.R. Ernst, J. Magn. Reson. 3, 10 (1970).
34. D. Ziessow and B. Blümich, Ber. Bunsenges. Phys. Chem. 78, 1169 (1974); B. Bliimich and D. Ziessow, J. Chem. Phys. 78, 1059 (1983).
35. B. Blümich, Bull. Magn. Reson. 7, 5 (1985).
36. J. Dadok and R.F. Sprecher, J. Magn. Reson. 13, 243 (1974).
37. R.K. Gupta, J.A. Ferretti, and E.D. Becker, J. Magn. Reson. 13, 275 (1974).
38. J.A. Ferretti and R.R. Ernst, J. Chem. Phys. 65, 4283 (1976).
39. B.L. Tomlinson and H.D.W. Hill, J. Chem. Phys. 59, 1775 (1973).
40. M.H. Levitt and R. Freeman, J. Magn. Reson. 33, 473 (1979).
41. M.H. Levitt, Prog. NMR Spectrosc. 18, 61 (1986).
42. R.L. Void, J.S. Waugh, M.P. Klein, and D.E. Phelps, J. Chem. Phys. 48, 3831 (1968).
43. R. Freeman and H.D.W. Hill, in *Dynamic NMR Spectroscopy* (eds. L.M. Jackman and F.A. Cotton), p. 131, Academic Press, New York, 1975.
44. S. Forsén and R.A. Hoffman, J. Chem. Phys. 39, 2892 (1963).
45. H.C. Torrey, Phys. Rev. 75, 1326 (1949); 76, 1059 (1949).
46. E.L. Hahn, Phys. Rev. 76, 145 (1949).
47. E.L. Hahn, Phys. Rev. 80, 297 (1950).
48. E.L. Hahn, Phys. Rev. 80, 580 (1950).
49. M. Emshwiller, E.L. Hahn, and D. Kaplan, Phys. Rev. 118, 414 (1960).
50. S.R. Hartmann and E.L. Hahn, Phys. Rev. **128**, 2042 (1962).
51. M.B. Comisarow and A.G. Marshall, Chem. Phys. Lett. **25**, 282 (1974) ibid 26, 489 (1974).
52. J.C. McGurk, H. Mäder, R.T. Hofmann, T.G. Schmalz, and W.H. Flygare, J. Chem. Phys. 61, 3759 (1974).
53. E.g. M.K. Bowman, in *Modern Pulsed and Continuous-Wave Electron Spin Resonance*, ed. L. Kevan and M.K. Bowman, p. 1, J. Wiley, New York, 1990.
54. M. Karplus, J. Chem. Phys. 30, 11 (1959).
55. J .H. Noggle and R.E. Schirmer, *The Nuclear Overhauser* Effect, Academic Press, New York, 1971.
56. K. Wüthrich, *NMR of Proteins and Nucleic Acids,* Wiley Interscience, New York, 1986.
57. S. Yatsiv, Phys. Rev. 113, 1522 (1952).
58. W.A. Anderson and R. Freeman, J. Chem. Phys. 37, 85 (1962).
59. R. Freeman and W.A. Anderson, J. Chem. Phys. 37, 2053 (1962).
60. R.A. Hoffman and S. Forsén, Prog. NMR Spectrosc. 1, 15 (1966).
61. J. Jeener, Ampere International Summer School, Basko Polje, Jugoslavia, 1971, unpublished.
62. R.R. Ernst, *VIth International Conference on Magnetic Resonance in Biological Systems,* Kandersteg, Switzerland, 1974, unpublished.
63. W.P. Aue, E. Bartholdi, and R.R. Ernst, J. Chem. Phys. 64, 2229 (1976).
64. J. Jeener, B.H. Meier, and R.R. Ernst, J. Chem. Phys. 71, 4546 (1979).
65. B.H. Meier and R.R. Ernst, J. Am. Chem. Soc. 101, 6641 (1979).
66. S. Macura and R.R. Ernst, Mol. Phys. 41, 95 (1980).
67. Anil Kumar, R.R. Ernst, and K. Wüthrich, Biochem. Biophys. Res. Commun. 95, 1 (1980).
68. M.P. Williamson, T.F. Havel, and K. Wüthrich, J. Mol. Biol. 182, 295 (1985).
69. A.D. Kline, W. Braun, and K. Wüthrich, J. Mol. Biol. 189, 377 (1986).
70. B.A. Messerle, A. Schaffer, M. Vasik, J.H.R. Kägi, and K. Wüthrich, J. Mol. Biol. 214, 765 (1990).
71. G. Otting, Y.Q. Qian, M. Billeter, M. Müller, M. Affolter, W.J. Gehring, and K. Wüthrich, EMBO J. 9, 3085 (1990).
72. T.F. Haveland and K. Wüthrich, Bull. Math. Biol. 46, 673 (1984).
73. W. Braun and N. Go, J. Mol. Biol. 186, 611 (1985).

74. R. Kaptein, E.R.P. Zuiderweg, R.M. Scheek, R. Boelens, and W.F. van Gunsteren, J. Mol. Biol. 182, 179 (1985).
75. G.M. Clore, A.M. Gronenborn, A.T. Brünger, and M. Karplus, J. Mol. Biol. 186, 435 (1985).
76. Y. Huang, S. Macura, and R.R. Ernst, J. Am. Chem. Soc. 103, 5327 (1981).
77. G.W. Eich, G. Bodenhausen, and R.R. Ernst, J. Am. Chem. Soc. 104, 3731 (1982).
78. P.H. Bolton and G. Bodenhausen, Chem. Phys. Lett. 89, 139 (1982).
79. Spectra recorded by C. Griesinger, see R.R. Ernst, Chimia 41, 323 (1987).
80. L. Braunschweiler and R.R. Ernst, J. Magn. Reson. 53, 521 (1983).
81. D.G. Davis and A. Bax, J. Am. Chem. Soc. 107, 2821 (1985).
82. A.A. Bothner-By, R.L. Stephens, J. Lee, C.O. Warren, and R.W. Jeanloz, J. Am. Chem. Soc. 106,811 (1984).
83. R. Brüschweiler, B. Roux, M. Blackledge, C. Griesinger, M. Karplus, and R.R. Ernst, J. Am. Chem. Soc. 114, 2289 (1992).
84. C. Griesinger, G. Otting, K. Wiithrich, and R.R. Ernst, J. Am. Chem. Soc. 110, 7870 (1988).
85. J. Briand and R.R. Ernst, Chem. Phys. Lett. 185, 276 (1991).
86. S. Vega, T.W. Shattuck, and A. Pines, Phys. Rev. Lett. 37, 43 (1976).
87. S. Vega and A. Pines, J. Chem. Phys. 66, 5624 (1977).
88. A. Wokaun and R.R. Ernst, Mol. Phys. 36,317 (1978).
89. L. Braunschweiler, G. Bodenhausen, and R.R. Ernst, Mol. Phys. 48, 535 (1983).
90. A. Bax, R. Freeman, and S.P. Kempsell, J. Am. Chem. Soc. 102, 4849 (1980).
91. A. Bax, R. Freeman, and S.P. Kempsell, J. Magn. Reson. 41, 349 (1980).
92. U. Piantini, O.W. Sørensen, and R.R. Ernst, J. Am. Chem. Soc. 104, 6800 (1982).
93. N. Müller, G. Bodenhausen, K. Wiithrich, and R.R. Ernst, J. Magn. Reson. 65, 531 (1985).
94. C. Radloff and R.R. Ernst, Mol. Phys. 66, 161 (1989).
95. A. Wokaun and R.R. Ernst, Chem. Phys. Lett. 52, 407 (1977).
96. G. Bodenhausen, H. Kogler, and R.R. Ernst, J. Magn. Reson. 58, 370 (1984).
97. M.H. Levitt and R.R. Ernst, Chem. Phys. Lett. 100, 119 (1983).
98. M.H. Levitt and R.R. Ernst, J. Chem. Phys. 83, 3297 (1985).
99. C. Griesinger, O.W. Sørensen, and R.R. Ernst, J. Am. Chem. Soc. 107, 6394 (1985).
100. C. Griesinger, O.W. Sørensen, and R.R. Ernst, J. Chem. Phys. 85, 6837 (1986).
101. C. Griesinger, O.W. Sørensen, and R.R. Ernst, J. Magn. Reson. 75, 474 (1987).
102. A. Bax and R. Freeman, J. Magn. Reson. 44, 542 (1981).
103. B.U. Meier and R.R. Ernst, J. Magn. Reson. 79, 540 (1988).
104. A.A. Maudsley and R.R. Ernst, Chem. Phys. Lett. 50, 368 (1977).
105. G. Bodenhausen and R. Freeman, J. Magn. Reson. 28,471 (1977).
106. L. Müller, J. Am. Chem. Soc. 101, 4481 (1979).
107. M. Ernst, C. Griesinger, R.R. Ernst, and W. Bermel, Mol. Phys. 74, 219 (1991).
108. M.H. Levitt, O.W. Sørensen, and R.R. Ernst, Chem. Phys. Lett. 94, 540 (1983).
109. H. Kogler, O.W. Sorensen, G. Bodenhausen, and R.R. Ernst, J. Magn. Reson. 55, 157 (1983).
110. H.D. Plant, T.H. Mareci, M.D. Cockman, and W.S. Brey, 27th Exp. NMR Conference, Baltimore, MA 1986.
111. G.W. Vuister and R. Boelens, J. Magn. Reson. 73, 328 (1987).
112. C. Griesinger, O.W. Sørensen, and R.R. Ernst, J. Magn. Reson. 73, 574 (1987).

113. C. Griesinger, O.W. Sørensen, and R.R. Ernst, J. Am. Chem. Soc. 109, 7227 (1987).
114. H. Oschkinat, C. Griesinger, P. Kraulis, O.W. Sørensen, R.R. Ernst, A.M. Gronenborn, and G.M. Clore, Nature (London) 332, 374 (1988).
115. G.W. Vuister, R. Boelens, and R. Kaptein, J. Magn. Reson. 80, 176 (1988).
116. C. Griesinger, O.W. Sørensen, and R.R. Ernst, J. Magn. Reson. 84, 14 (1989).
117. E.R.P. Zuiderweg and S.W. Fesik, Biochemistry 28, 2387 (1989).
118. D. Marion, P.C. Driscoll, L.E. Kay, P.T. Wingfield, A. Bax, A.M. Gronenborn, and G.M. Clore, Biochemistry 28, 6 150 (1989).
119. S. Boentges, B.U. Meier, C. Griesinger, and R.R. Ernst, J. Magn. Reson. 85, 337 (1989).
120. O.W. Sørensen, J. Magn. Reson. 89, 210 (1990).
12 1. L.E. Kay, G.M. Clore, A. Bax, and A.M. Gronenborn, Science 249,411 (1990).
122. Z.L. Mádi, C. Griesinger, and R.R. Ernst, J. Am. Chem. Soc. 112, 2908 (1990).
123. R. Brüschweiler, M. Blackledge, and R.R. Ernst, J. Biomol. NMR 1, 3 (1991).
124. W. Burgermeister, T. Wieland, and R. Winkler, Eur. J. Biochem. 44, 311 (1974).
125. H. Kessler, M. Klein, A. Müller, K. Wagner, J.W. Bats, K. Ziegler, and M. Frimmer, Angew. Chem. 98, 1030 (1986); H. Kessler, A. Müller, and K.H. Pook, Liebig Ann. Chem. 903 (1989); H. Kessler, J.W. Bats, J. Lantz, and A. Müller, Liebig Ann. Chem. 913 (1989); J. Lantz, H. Kessler, W.F. van Gunsteren, H.J. Berendsen, R.M. Scheek, R. Kaptein, and J. Blaney, Proc. 20th Eur. Pept: Symp. 1989, p. 438 (Ed. G. Jung, E. Bayer).
126. R.R. Ernst, M. Blackledge, S. Boentges, J. Briand, R. Brüschweiler, M. Ernst, C. Griesinger, Z.L. Mádi, T. Schulte-Herbrüggen, and O.W. Sorensen, in *Proteins, Structure, Dynamics, Design,* ed. V. Renugopalakrishnan, P.R. Carey, I.C.P. Smith, S.G. Huang, and A.C. Storer, ESCOM, Leiden, 1991.
127. P.C. Lauterbur, Nature 242, 190 (1973).
128. Anil Kumar, D. Welti, and R.R. Ernst, J. Magn. Reson. 18, 69 (1975).
129. W.A. Edelstein, J.M.S. Hutchison, G. Johnson, and T.W. Redpath, Phys. Med. Biol. 25, 751 (1980).
130. P. Mansfield, A.A. Maudsley, and T. Baines, J. Phys. E9, 271 (1976).
131. P.C. Lauterbur, D.M. Kramer, W.V. House, and C.-N. Chen, J. Am. Chem. Soc. 97, 6866 (1975).